Copyright Warning & Restrictions

The copyright law of the United States (Title 17, United States Code) governs the making of photocopies or other reproductions of copyrighted material.

Under certain conditions specified in the law, libraries and archives are authorized to furnish a photocopy or other reproduction. One of these specified conditions is that the photocopy or reproduction is not to be "used for any purpose other than private study, scholarship, or research." If a, user makes a request for, or later uses, a photocopy or reproduction for purposes in excess of "fair use" that user may be liable for copyright infringement,

This institution reserves the right to refuse to accept a copying order if, in its judgment, fulfillment of the order would involve violation of copyright law.

Please Note: The author retains the copyright while the New Jersey Institute of Technology reserves the right to distribute this thesis or dissertation

Printing note: If you do not wish to print this page, then select "Pages from: first page # to: last page #" on the print dialog screen

NJIT
New Jersey's Science & Technology University

The Van Houten library has removed some of the personal information and all signatures from the approval page and biographical sketches of theses and dissertations in order to protect the identity of NJIT graduates and faculty.

ABSTRACT

DEVELOPMENT OF AN ION SOURCE FOR IMPLANTATION OF DECABORANE

by
Ravidath Gurudath

Future generations of Si technology will require ultra shallow junctions (tens of nm) in the drain and source regions of MOS transistors. Fabrication of such shallow p-type junctions requires implantation of boron at ultra low energies ($\cong$1keV), below the limits of standard ion implantation technology. A proposed solution involves implantation of $B_{10}H_x^+$ ions in which boron atoms carry less than 10% of the beam energy. Thus shallow implantation may be possible with standard ion implanters operating at tens of kV.

This thesis is a part of the feasibility study of this novel technology. The ionization of decaborane ($B_{10}H_{14}$) under different electron impact energies and temperature was investigated by ion mass spectroscopy. It was found that the molecule is more robust than expected and that most of the generated ions contained ten boron atoms. An electron impact ion source was designed and its operation simulated using an ion optics program SIMION. Based on the simulation results, an experimental ion source was constructed and its operating characteristics were measured with argon. Experimental ion beam extraction and focussing conditions are in agreement with simulations. The source will be a part of an experimental ion implantation system being built at the Ion Beam and Thin Film Research Laboratory at NJIT.

DEVELOPMENT OF AN ION SOURCE FOR IMPLANTATION OF DECABORANE

by
Ravidath Gurudath

A Thesis
Submitted to the Faculty of
New Jersey Institute of Technology
in Partial Fulfillment of the Requirements for the Degree of
Master of Science in Electrical Engineering

Department of Electrical and Computer Engineering

May 1999

APPROVAL PAGE

DEVELOPMENT OF AN ION SOURCE FOR IMPLANTATION OF DECABORANE

Ravidath Gurudath

Dr. Marek Sosnowski, Thesis Advisor — Date
Assoc. Professor, Department of Electrical and Computer Engineering, NJIT.

Dr. Durga Misra, Committee Member — Date
Assoc. Professor, Department of Electrical and Computer Engineering, NJIT.

Dr. John Poate, Committee Member — Date
Department of Physics, NJIT.

Dr. Dale Jacobson, Committee Member — Date
Bell Laboratories-Lucent Technologies, Murray Hill NJ.

BIOGRAPHICAL SKETCH

Author: Ravidath Gurudath

Degree: Master of Science

Date: May 1999

Undergraduate and Graduate Education:

- Master of Science in Electrical Engineering,
  New Jersey Institute of Technology, Newark, NJ. 1999

- Bachelor of Engineering in Electrical & Electronics Engineering,
  Rashtreeya Vidyalaya College of Engineering, Bangalore, India, 1996.

Major: Electrical Engineering

This thesis is dedicated to my

beloved parents

ACKNOWLEDGMENT

Words are not sufficient to express my deep sense of gratitude to Dr. Marek Sosnowski, who not only served as my research supervisor, providing valuable and countless resources, insight and intuition, but also constantly gave me support, encouragement, and reassurance. I am grateful to him for providing me the opportunity to work under his supervision during my graduate study at NJIT.

I would also like to thank Dr.'s John Poate, Dale Jacobson and Durga Misra for serving as members of the committee. I am grateful to Dr. Dale Jacobson and Tony Mujsce of Bell Laboratories for their technical assistance during this work.

Special appreciation goes to Ed Oksienik for his help in machining components of the system. My fellow students at the Ion Beam and Thin Film Research Laboratory, Mathew Weltman, Maria Albano and Anamika Patel are deserving of recognition for their support.

TABLE OF CONTENTS

Chapter	Page
1. INTRODUCTION	1
2. IONIZATION OF DECABORANE	5
2.1 Ionization Techniques	5
2.1.1 Electron Impact Ionization	7
2.2 Measurement of Ionization Properties of Decaborane	9
2.2.1 Experimental Setup	9
2.2.2 Measurements	11
2.3 Analysis of the Spectra	12
2.3.1 Hydrogen Dissociation	13
2.3.2 Boron Dissociation	14
2.3.2.1 Electron Energy Dependence	14
2.3.2.2 Temperature Dependence	18
3. ION SOURCE DESIGN	19
3.1 Design Criteria for the Ion Source System	19
3.2 Electron Impact Source Based on Bayard-Alpert Gauge	20
3.2.1 The Ionizer	21
3.2.2 Ion Extraction System	23
3.3 Simulation of the Electron Impact Source using SIMION	24
3.3.1 Preliminary Design	26

TABLE OF CONTENTS
(Continued)

Chapter	Page
3.3.2 Modifications	29
3.3.3 Final Design	30
3.3.4 Summary of Simulation Results	33
3.4 Description of the Ion Source Structure	34
3.4.1 The Source Flange	35
3.4.2 The Ionizer	36
3.4.3 The Electrode Assembly	37
3.4.4 Electrical System for the Ion Source	40
4 MEASUREMENTS OF CHARACTERISTICS OF THE ION SOURCE	41
4.1 Ionizer Filament Characteristics	41
4.1.1 Problems Faced during Initial Ionizer Operation and their Solutions	43
4.2 Ion Current Measurements	48
4.2.1 Ion Current Measurement using Concentric Apertures	49
4.3 Simulation vs. Experimental Results	51
5 MASS SEPARATION AND ION BEAM TRANSPORT SYSTEM	53
6 CONCLUSIONS	58
APPENDIX A DECABORANE	59
APPENDIX B CALCULATION OF ISOTOPE DISTRIBUTION OF $B_{10} H_{14}$	62
REFERENCES	63

LIST OF TABLES

Table		Page
3.1	Summary of simulation results	33
3.2	List of parts used for ionizer construction	37
4.1	Ionizer filament characteristics with the first version of the ionizer	42
4.2	Ionizer filament characteristics with filament 1	45
4.3	Ionizer filament characteristics with filament 2	46
4.4	Ionizer filament characteristics with filament 1 & 2 in series	47
4.5	Preliminary ion current data	49
4.6	Ion current measurements using concentric apertures	50
B1	Isotope distribution of $B_{10}H_{14}$	62

LIST OF FIGURES

Figure		Page
2.1	Experimental setup to obtain mass spectra of decaborane.................	9
2.2	Mass spectrum of decaborane at 70eV, 250°C..............................	11
2.3	Mass spectrum of decaborane based on isotope distribution................	13
2.4	Normalized mass spectra at 25eV, 70eV, 255eV, 250°C....................	15
2.5	Abundance of $B_{10}H_x$ ions vs. Electron energy...............................	16
2.6	Relative abundance of $B_{10}H_x$ ions vs. Electron energy......................	17
2.7	Relative abundance of $B_{10}H_x$ ions vs. Temperature..........................	18
3.1	Bayard-Alpert gauge...	20
3.2	Preliminary design of the ion source...	26
3.3	Beam focussing under different electrode potentials.........................	27
3.4	Ions generated farther from extraction electrode unable to be extracted..	28
3.5	Modified version...	29
3.6	Final version of the source in 2D and 3D views..............................	31
3.7	Beam focussing at various starting locations................................	32
3.8	Source end of the beamline..	34
3.9	The Source flange...	35
3.10	The Ionizer structure..	38
3.11	The Electrode assembly..	38
3.12	The Ion source...	39
3.13	Schematic of the electric connections..	40
4.1	Ionizer filament emission characteristics.....................................	42

LIST OF FIGURES
(Continued)

Figure		Page
4.2	Ionizer filament emission characteristics with filament 1..................	45
4.3	Ionizer filament emission characteristics with filament 2..................	46
4.4	Ionizer filament emission characteristics with filament 1 & 2 in series...	47
4.5	Ion current measurements using concentric apertures........................	49
4.6	Simulations vs. Experimental data..	52
5.1	Beamline..	54
5.2	Illustration of the analyzer magnet operation..................................	55
5.3	Quadrupole..	57
A1	Structure of the decaborane molecule..	59
B1	Isotope distribution of $B_{10}H_{14}$..	62

CHAPTER 1
INTRODUCTION

The growth of semiconductor IC industry over the past three decades has been fueled by continued shrinking of transistors to ever smaller dimensions for higher packing density, faster circuit speeds and lower power dissipation. These advances led to computers and networks with far superior performance and dramatically reduced cost per function today. The trend is expected to continue beyond the year 2000 when 0.1micron generation technology will be in production [1]. The key challenge of the present day technology is the development of fabrication systems that can meet this requirement [2].

Ion implantation has played a critical role in the development of semiconductor technology over the past 25 years. It has been the primary technology for doping of semiconductors to form devices and VLSI circuits. The advantages of ion implantation include the purity of implanted species achieved by magnetic mass separation, the control of implantation depth by choice of ion energy and accuracy of the dose and uniformity across the wafer achieved by beam current measurement. Whether the process technology is MOS, Bipolar, merged processes such as BiCMOS, or GaAs, ion implantation is essential for the production of economically competitive solid state devices and integrated circuits. Scaling of CMOS is defined by the transistor gate width. Recent advances of growth of CMOS fabrication technology have led to the production of 180nm devices and presently, the development of 120nm devices. Technology for the 100nm devices is in the research stage. Scaling of MOS devices requires reduction of transistor lateral and vertical dimensions. This requires creation of very shallow junctions in the source, drain and the source drain extension regions.

Today's most challenging doping application is formation of extremely shallow junctions [3]. Although less of a problem for n-channel transistors, where the n-type source/drains are heavily doped with phosphorus or arsenic, it is a potentially major problem for p channel devices where the source/drains are heavily doped with boron. The reason is that boron atoms are light and therefore their projected range in Si is much larger. For shallow implantation, they must be accelerated to very low energies. Generation and transport of ion beams at low energies is hindered by Coulomb forces and the attainable current becomes so small as to be impractical for semiconductor implantation [4], [5].

Presently this problem is solved by the use of BF_2 ions, which are heavier than elemental boron ions, allowing a higher energy to be used (about 5 times higher) for the same implant depth. Fluorine however is corrosive and can create voids in silicon, attack gate oxides and metal and enhance diffusion in gates. It is a problem particularly in thin gate oxides and small devices. Thus, pure boron is favored although sub-keV implant energies are required for shallow junction formation.

New techniques for future generation technology are being investigated to solve this problem, include schemes based on deceleration of energetic beams in front of the target, plasma immersion technique etc [6]. Although implanters based on the deceleration technique have become recently available, their usefulness in semiconductor fabrication process is still being tested. Plasma immersion techniques do not discriminate among various ion species and their potential for precise semiconductor doping remains uncertain. An alternative technique currently being developed, is cluster or molecular implantation [7].

A cluster of n atoms impacting on a surface with kinetic energy E can be viewed as an impact of n atoms with energy E/n. For example, a cluster of a hundreds atoms and a kinetic energy of a hundred keV has one keV per each constituent atom. Another important aspect of ionized clusters is their high mass to charge ratio. Thus an n atom cluster transports n times the mass of a monomer beam at the same current. The space charge problems in the beam transport as well as problems of target charging are minimized. These effects make cluster ion implantation an attractive alternative for shallow junction formation.

It has been recently demonstrated at the Kyoto University, Japan that MOS devices with ultra shallow junctions have been formed using molecular ions of decaborane [8], [9]. Decaborane molecule consists of ten Boron atoms and 14 Hydrogen atoms, therefore the boron atoms in the molecular beam carry approximately $1/11^{th}$ of the beam energy and the boron dose per unit charge is ten times larger than in the case of monomer B ion beam. This has aroused great interest in the implantation community for the possible use of decaborane as implant specie. But attempts to use decaborane in conventional implanters have not been successful till now because the $B_{10}H_{14}$ molecule dissociates in plasma generated by most ion sources. Thus, new systems that can generate and handle such beams are needed.

This thesis contains information pertaining to the work carried out at the Ion Beam and Thin Film Research Laboratory at NJIT on the decaborane ion implantation. The main objectives of the work were

a) To investigate the feasibility of generating ion beams of decaborane.

b) To develop a research implantation system for decaborane ions.

The work included design of an experimental ion source and implantation system, experimental data on ionization of decaborane, the source construction and measurement of its characteristics.

The basic principles of ionization and the experiments conducted to determine the ionization behavior of decaborane by ion mass spectroscopy are discussed in chapter two.

The third chapter describes the development of an ion source. The design of an electron impact source, the simulations carried out to determine the operating conditions of the ion source (using an ion optics program SIMION) and details regarding source construction, are discussed here.

Chapter four contains data on the basic characteristics of the experimental ion source. Ion current measurements using argon and the comparison of the beam extraction and focussing conditions with simulations are presented here.

The ion source will be a part of an experimental ion implantation system being built at NJIT. The description of this system is included in chapter five.

A summary of the results obtained so far on possible use of decaborane as ion source material for Boron implantation is presented in chapter six.

Appendix A contains data on the physical and chemical properties of decaborane and safety measures to be taken when handling it.

Appendix B contains the calculation of the isotope distribution of $B_{10}H_{14}$.

CHAPTER 2

IONIZATION OF DECABORANE

The nature of ion species determines to a great extent, the conditions needed for efficient source operation. There was no available data on the ionization of decaborane, whose properties as implant specie were being investigated. There was a particular concern about the stability of the molecule under conditions of excessive temperatures and at high electron energies because we learned that attempts to generate decaborane ion beam in standard ion implanter sources were not successful. Therefore, we have conducted experiments to determine the ionization properties of the decaborane molecules, which were to be used in the design of the ion source.

The first section of this chapter describes the various techniques of creating ions. In the second section, the experiments conducted to measure the mass spectra of decaborane ions generated by electron impact ionization and measurement details are presented. In the third section, analysis and interpretation of these spectra are discussed.

2.1 Ionization Techniques

An ion is an atom that has an excess or deficiency of electrons and is, hence, electrically charged. Some of the principal ways in which ions can be produced are electron impact ionization, surface ionization, photoionization, field ionization, and chemical ionization.

- *Electron impact ionization*

In electron impact ionization, ions are produced by the electron bombardment of a gas or vapor of the material to be ionized. Electron bombardment can be achieved in several

ways such as arc discharge, r.f. discharge, a confined electron cloud etc. Most ion species can be created by this method.

- *Surface Ionization Process*

For metals having low ionization potentials such as alkali metals and rare earths, surface ionization can be used for the generation of ions directly from hot metal surfaces with which neutral metal atoms come into contact.

- *Photoionization*

A photon can cause ionization if its energy hν exceeds the ionization energy eV_i of an ionizable particle. Ultraviolet light, x-rays, and gamma rays are the best producers of elemental ions by photoionization. Because the ion currents derivable from photoionization are smaller than from other techniques, practical ion sources do not use this phenomenon.

- *Field Ionization*

Field ionization is the process whereby atoms or molecules adsorbed on or passing near to a surface, usually a sharp point, are ionized by a high electric field at the surface.
This scheme is not widely used because it is practical only for certain ionic species and the attainable ion current is limited.

- *Chemical Ionization (CI)*

Chemical ionization (CI) of a gas occurs through interaction with reactive ions or exited molecules. CI generally yields much less fragmentation of the neutral molecules than Electron Impacts and is considered a low energy or "soft" ionization method.

Our choice of the type of ionization process for decaborane was based on the requirements that the process should generate predominantly $B_{10}H_{14}$ ions i.e. the ionization process should not result in substantial break up of B_{10} cluster Since break up of the large molecule was expected to occur due to impact of energetic electrons and high temperatures, both of these parameters should be controlled.

Electron Impact Ionization is one process wherein the energy of the electrons could be varied by adjusting the potential difference between the anode and cathode, thereby providing control over the ionization process. Other ionization techniques do not provide any direct means of controlling electron energy, which determines the ionization and dissociation rates. We have learned that attempts to obtain $B_{10}H_x$ ions from standard implanter sources operating with energetic arc discharge were not successful. Thus, EI ionization was chosen as the technique to ionize decaborane.

2.1.1 Electron Impact Ionization

Electrons in passing through a gas, can lose energy by means of elastic collisions, ionizing collisions, dissociation of gas molecules and excitation of the gas atoms or molecules. For sufficient initial electron kinetic energy, the amount of energy transferred to the atom should exceed the ionization energy eV_i where V_i is the ionization potential of the atomic species involved [10]. When the incident electron has energy in excess of the ionization energy, the excess energy can appear in several ways viz. as kinetic energy of the ejected electron, or as multiple ionization of the gas particle or a combination of these effects. It is highly probable that either the primary or the secondary electron will emerge with most of initial energy following a collision. For efficient ionization, the

electron density should be high, so that many collisions can occur. However at electron energies sufficiently exceeding ionization potential, the ionization probability decreases [11]. The rate of ion production in an electron impact ion source depends on a number of factors such as:

- The ionization cross-section for collisions.

The cross section for ionization of an atom or a molecule expresses the probability of ionization in a collision with an electron. It is related to the effective size of the molecule and depends on the impact energy. The radius of decaborane molecule is obviously larger than that of an individual Boron atom. Since decaborane molecule is larger than boron atom, one can expect its ionization cross section to be much greater than that of single atom. Ionization cross section depends also on the impact energy and is related to the uniform potential.

- Electron Path Length – Magnetic field confinement

It is considerably more efficient to reuse electrons for ionization many times, rather than having to create them afresh from neutral atoms and then heat them starting from low energy each time. Primary electron confinement can be assisted in a number of ways. The electrons can be caused to reflect forward and backward between negatively biased electrodes while tied to an axial-magnetic field; the electrons can be confined to a magnetic mirror; by appropriate modification of electrode structure and applied voltages.

- The creation and loss of electrons.

The electron density in the ionization chamber is dependent on the relative values of the creation and loss rates of the electrons.

2.2 Measurement of Ionization Properties of Decaborane

2.2.1 Experimental Setup

In order to understand the effects of electron impacts on the decaborane molecule, we have performed a series of measurements of mass spectra of ions generated by electron impact in the 20eV-255eV range and source temperatures upto 350°C.

An experiment was setup as shown in Fig 2.1

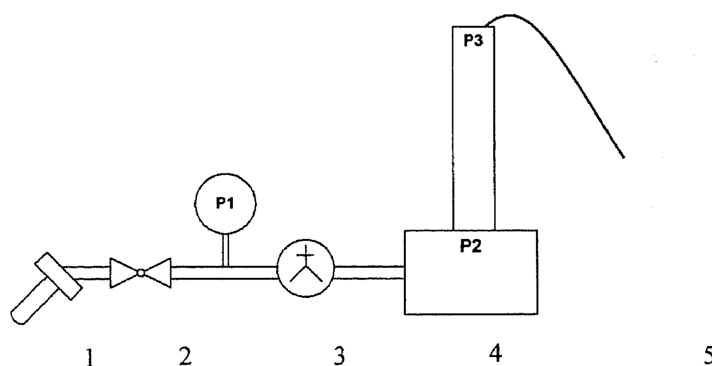

Fig 2.1 Experimental setup to obtain mass spectra of decaborane.

1 : Glass Ampoule enclosing small amount of Decaborane
2 : Inlet Valve
3 : Needle Valve
4 : Mass Spectrometer
5 : Data Acquisition System
P1, P2 P3 : Pressures gauges in different ports of the system.

A small amount (< $0.1cm^3$) of decaborane enclosed in a glass ampoule was placed at one end of the system separated by an inlet (ON/OFF) valve. A needle valve controlled the amount of decaborane let in to the ionizer, which was a part of the mass spectrometer system.

The mass spectrometer system consists of the following:

- Electron impact source
- Quadrupole mass analyzer
- Detector
- Control and data acquisition system

Positive ions are produced from the vapor of the sample in the ion source followed by electron impact ionization (EI). The ions are accelerated to a quadrupole mass analyzer and detected by an electron multiplier. The analyzer acts as a mass filter admitting to the detector only ions of a specific mass. The analyzer settings are secured over a preset mass range while the detector signal is recorded. The resulting mass spectra are stored on a computer, which also controls the system. Its software '*HP G1034C MS ChemStation*' is written in a high level language to simplify updating and to make it easier for customizing specific process requirements.

The setup described above used a differential pumping system with different pressures in its main sections. P1 is the pressure in the port before the inlet to the ion source, P2 is the ion source pressure and P3 is the pressure in the quadrupole analyzer and detector port. In our experiment, P1 was equal to the sublimation pressure of decaborane (15-20mT), P2 was in the 10^{-6} T range, and P3 the pressure in the analyzer was at a much still lower pressure

2.2.2 Measurements

Decaborane, which is a solid at room temperature, but sublimes easily (0.15 T at 20° C), was introduced as vapor to the ionizer. With the ionizer temperature maintained at 210°C, a series of measurements of mass spectra of ions generated by impact of electrons at 20eV, 70eV, 160eV, 200eV and 255eV were performed. Similar measurements were made at two other source temperatures viz. 250°C and 350°C. Each run was of 1min duration, a typical mass spectrum of decaborane at 70 eV and 250°C is shown in Fig 2.2.

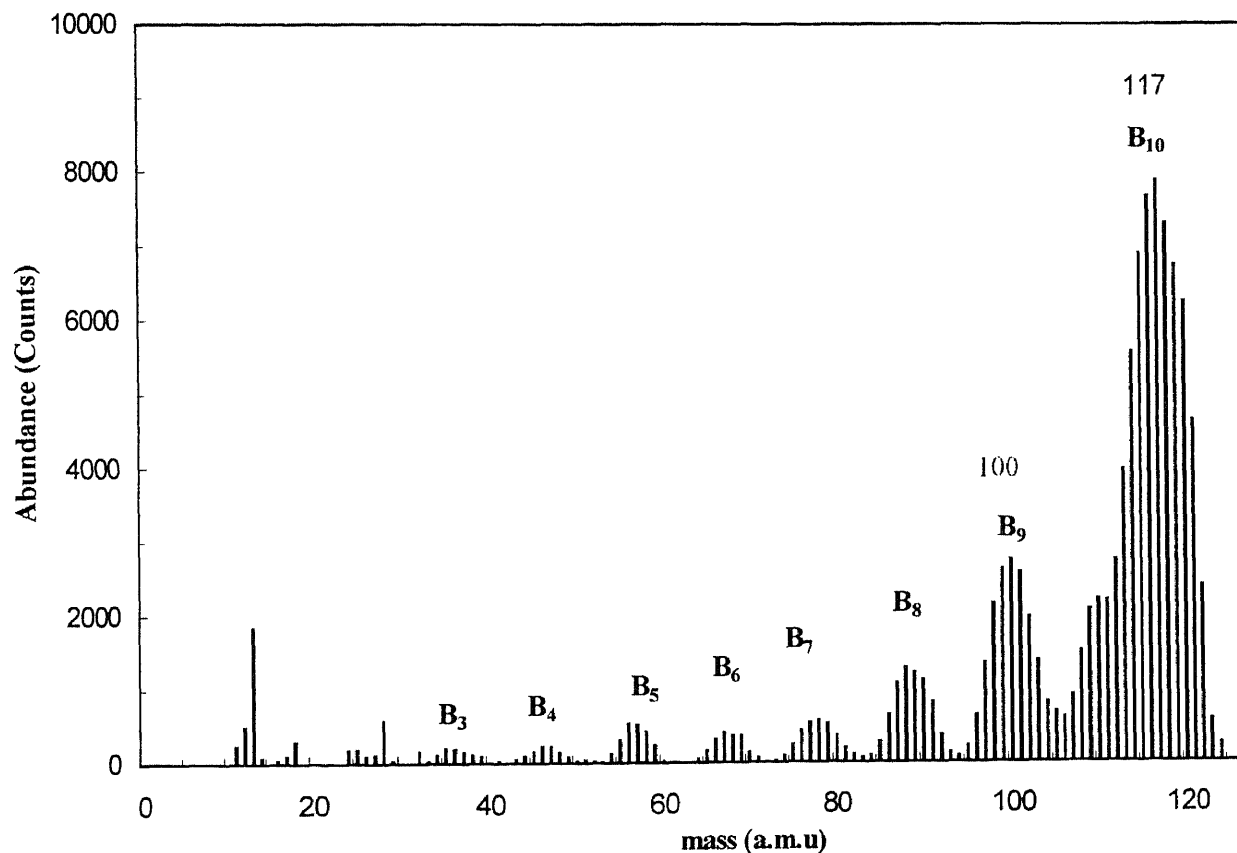

Fig 2.2 Mass Spectrum of Decaborane at 70 eV , 250°C

In the spectra shown in Fig 2.2, the spectral lines observed correspond to fragments of ions of the original molecule with a different number of B atoms. The fine structure is due to the isotopic distributions of the atoms in the molecular ions and to different number of Hydrogen atoms in the fragments. There are two isotopes in natural boron, ^{10}B and ^{11}B with the ratio of 19% ^{10}B and 81% ^{11}B [12]. Using this information and the fact that hydrogen atoms can easily dissociate from the molecule, the form of the observed spectra can be explained.

2.3 Analysis of the Spectra

Referring to the spectra in Fig 2.2, we observe groups of lines with decreasing order of the intensities from the right to the left (labeled as B_{10}, B_9, B_8, B_7, B_6, $B_{5...}$). In the first order approximation, it can be stated that each group contains different number of B atoms from right to the left 10,9,8...etc. There are ten such groups located at masses with difference of approximately 11 units. The right most group is of the highest intensity and lies between the masses 106 and 124. Therefore ions corresponding to these masses possibly arise from a combination of ($B_{10}H_{x\,(1<x<14)}$ + $B_9H_{x\,(7<x<14)}$) fragments. Since the intensity of the right most peak which includes masses contributed by $B_{10}H_x$ (110 to 124) is higher than that of the next group B_9H_x (106 to 113), it can be concluded that this group predominantly contains $B_{10}H_x$ ions. Similarly other groups in the spectrum could be assumed to be a combination of fragments (e.g. B_9H_x + B_8H_x and so on), they mostly consists of ions as labeled in the figure.

As ion groups with high masses, particularly B_{10}, are of greater interest to us than ions with lower masses, a more close analysis on the high-mass groups is in order. To

determine the exact content in these fragments, a mass spectrum of $B_{10}H_{14}$ based on the natural isotope ratio was generated using the binomial probability distribution [App B]. Here it is assumed that none of the hydrogen molecules are lost during ionization. This isotopic distribution appears as shown in the Fig 2.3. The relative abundance for groups B_9H_{14}, B_8H_{14}... have been scaled arbitrarily for comparison purposes

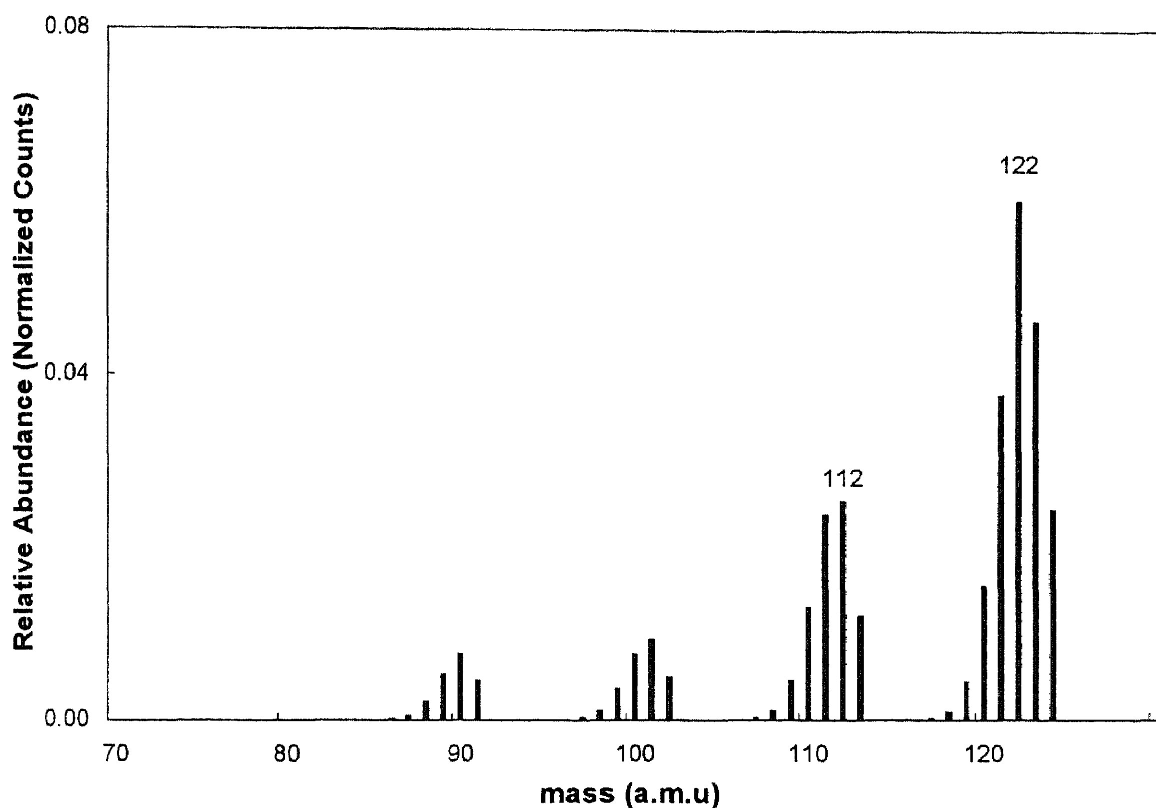

Fig 2.3 Mass spectrum of decaborane based on isotope distribution

2.3.1 Hydrogen Dissociation

Comparing the measured spectra (Fig 2.2) with the isotopic distribution (Fig 2.3), we observe that in the measured spectra, the $B_{10}H_x$ peak is at 117 a.m.u (116 at some electron energies) as opposed to 122 observed in the isotopic distribution. This clearly

tells us that there is a loss of 5-6 Hydrogen atoms during ionization. Subsequent peaks viz. B_9H_x, B_8H_x...etc are of the form $B_yH_{(1 \text{ or } 2)}$.

2.3.2 Boron Dissociation

As mentioned earlier, maximizing the yield of ions having high masses from the ion source is of prime concern and the mass spectra indicates the abundance of these ions under different ionization conditions. The abundance of ions containing 10 boron atoms was analyzed as a function of electron-input energy and decaborane vapor temperature.

2.3.2.1 Electron Energy Dependence: Fig 2.4 shows the normalized mass spectra at three electron impact energies: 25eV, 70eV and 255eV. The normalization procedure consists of dividing all the line intensities (counts) by the sum of all the counts in the mass range 10 to 124. The reason for not including lower masses in the normalization procedure was the presence of source impurities not related to the decaborane. Mass spectrum at the lowest electron energy of 25eV had a large $B_{10}H_x$ peak and very small peaks corresponding to B_9H_x, B_8H_x...fragments. As the electron energy was increased to 70eV, all the peaks appeared with intensities increasing with B content. (Fig 2.4b). As the electron energies were increased beyond 100eV, the intensities of the low mass peaks started diminishing so that, at 255eV the spectrum resembled more that at 20eV than at 70eV.

It is also to be observed that there exits a shoulder on the left hand side of the $B_{10}H_x$ peak at 70eV which is absent in the other two spectra. This shoulder along with the smaller peaks suggests that the dissociation is higher at 70eV than at 20eV or at 255eV.

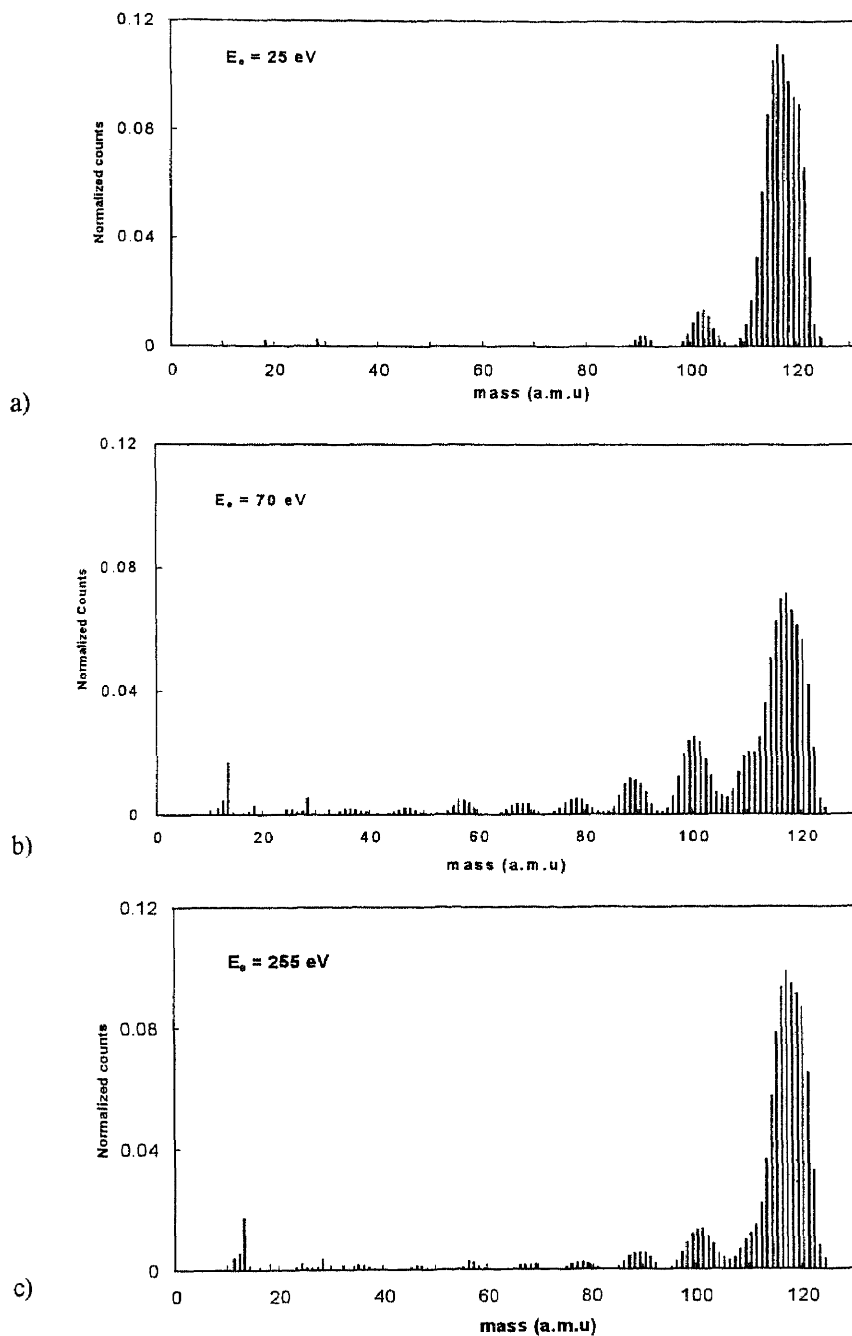

Fig 2.4 Normalized mass spectra at 25eV, 70eV and 255eV, 250°C

The plot in Fig 2.5 summarizes the absolute intensity at the right most peak in the spectra (denoted by $B_{10}H_x$) obtained in 18 different measurements 25eV to 255eV at 250°C source temperature. All spectra were accumulated for 1 min under stable pressure P1. The stability of the operation can be assessed by comparing measurements at the same conditions, taken at different times.

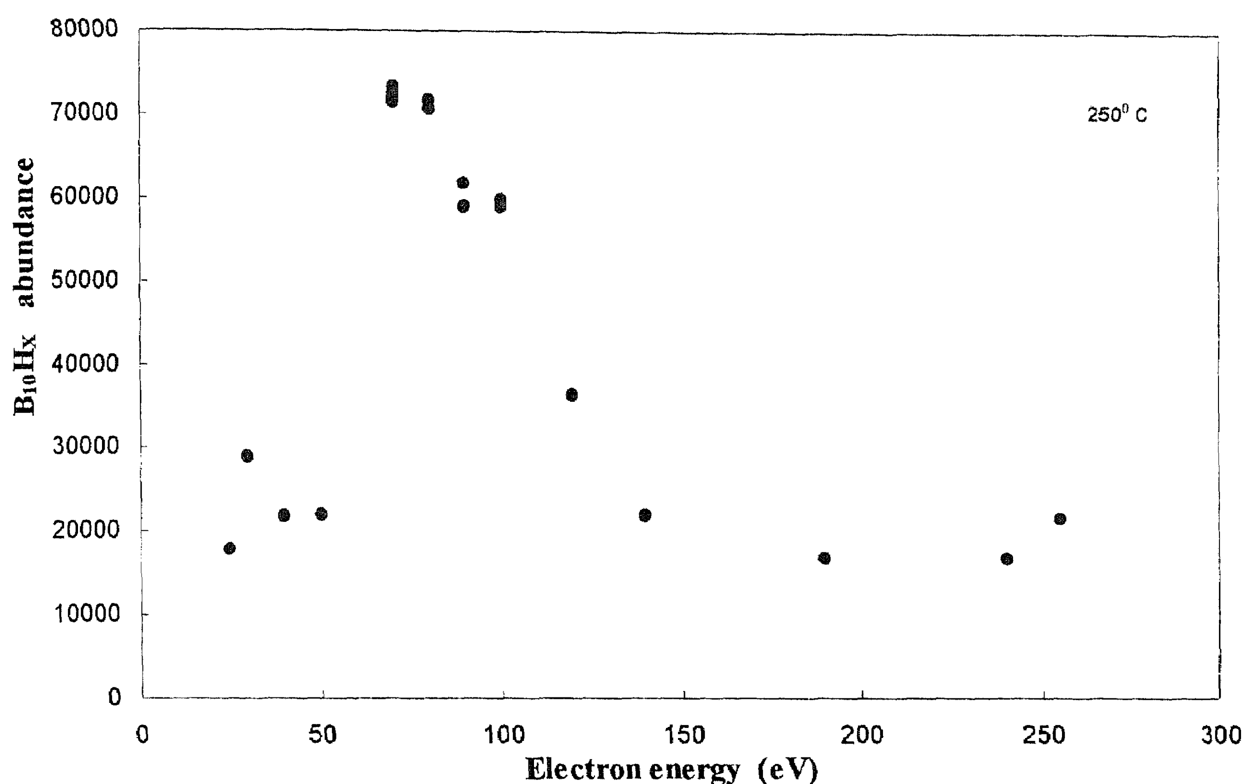

Fig 2.5 Abundance of $B_{10}H_X$ ions vs. Electron energy

The plot resembles the characteristic electron impact ionization cross section of many gases [11]. $B_{10}H_x$ ion intensity increases as a function of electron energy and reaches a maximum in the 70-100eV range. Beyond 100eV, the intensity decreases and the dissociation follows a similar but less steep energy dependence curve.

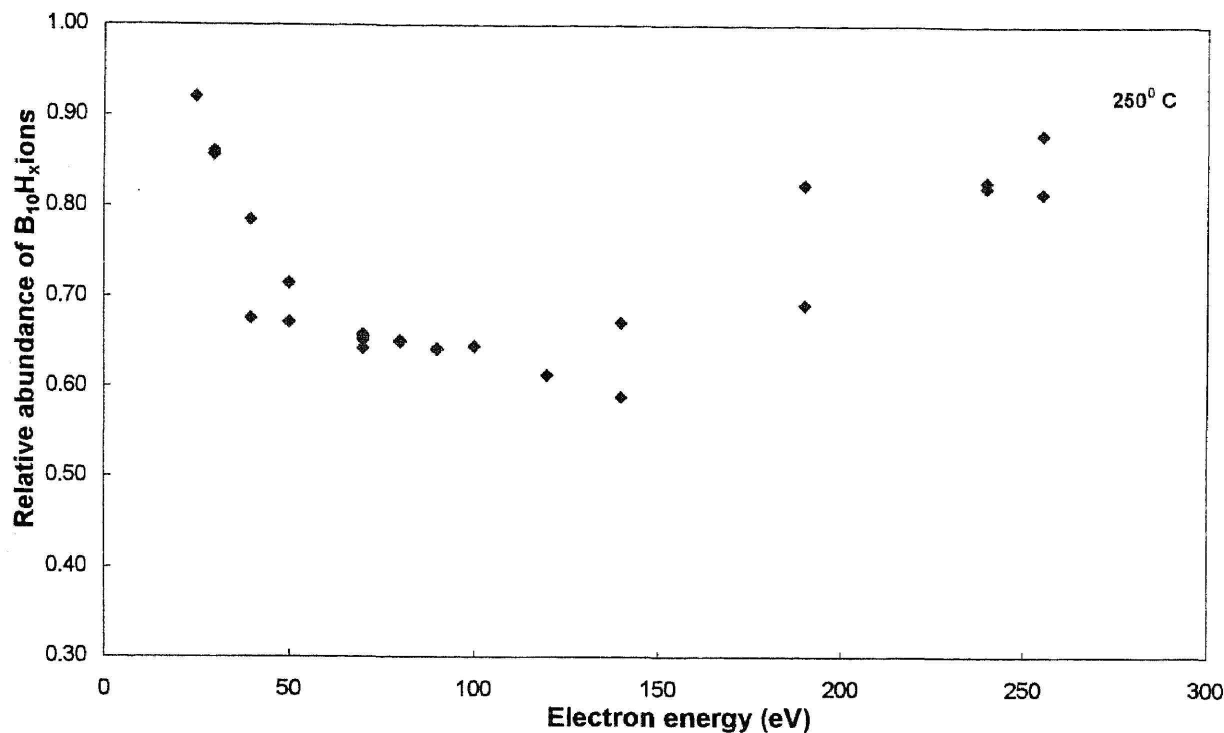

Fig 2.6 Relative abundance of $B_{10}H_x$ ions vs. Electron energy

The plot shown in Fig 2.6 shows the relative intensity of $B_{10}H_x$ ions at various electron energies. The relative intensity is the ratio of the $B_{10}H_x$ counts to the total number of counts (ions of masses>10) in the spectrum. This plot shows that while relative B_{10} intensity decreases initially with increasing electron impact energy, reaching a minimum at about 70eV, the dissociation of B_{10} cluster into smaller fragments does not vary appreciably with electron energy and that almost 70-95 % ions contain ten B atoms.

2.3.2.2 Temperature Dependence: To ascertain the stability of B_{10} cluster at higher temperatures, the ionizer temperatures was increased upto 350°C. A graph of $B_{10}H_x$ relative intensity versus temperature was plotted as in Fig 2.7. As seen from the plot, there was a marginal change in the relative intensity of B_{10} intensity at higher temperatures, except at 20eV. The higher effect of the temperature at the lowest electron current energy may be interpreted by the fact that dissociation of the molecule by electron impact is low, so that the temperature effect is more significant.

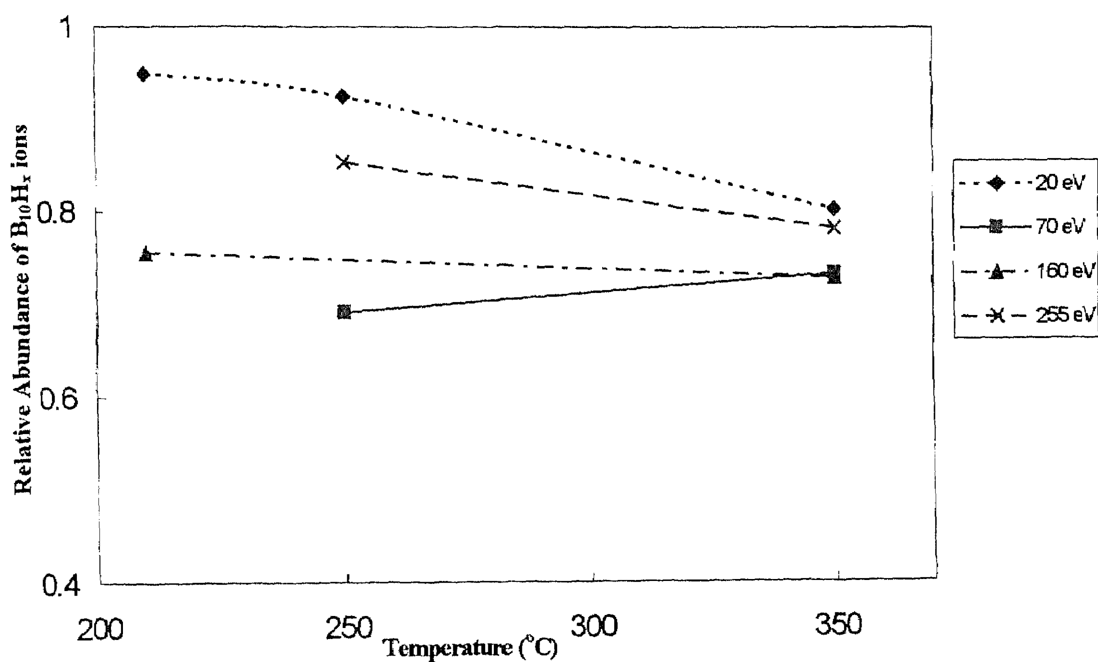

Fig 2.7 Relative abundance of $B_{10}H_x$ ions vs.Temperature

CHAPTER 3

ION SOURCE DESIGN

In chapter two, it was shown that decaborane molecule could be ionized effectively by electron impacts. The next step was to develop a system that generated these ions, extract them from the region where they are produced and then focus them to form the desired beam. This chapter describes the basic design of the ion source including the ionizer and the ion extraction assembly. Simulations were carried out to determine electrode geometry and potentials using an ion optics program SIMION [13] and finally, the construction of an experimental ion source system is described.

3.1 Design Criteria for the Ion Source System

With any design project, one is faced with a list of performance requirements that must be achieved. The experimental source was designed to study the ionization of decaborane and properties of the generated ion beams. The main design requirements were:

- Adjustable electron energies for maximizing the $B_{10}H_x$ ion current.
- Low Source temperature ($\leq 300°C$) to prevent dissociation of decaborane.
- Sufficient ion current ($\geq 1\ \mu A$) for ion implantation experiments.

3.2 Electron Impact Source Based on Bayard-Alpert Gauge.

The structure of the commercially available ion gauge of the Bayard-Alpert (B-A) type (Fig 3.1) is well suited for conversion into a simple source [14].

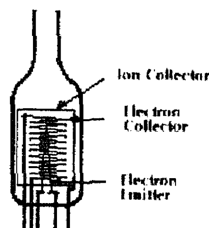

Fig 3.1 Bayard-Alpert gauge

The pressure of the ambient gas is determined by measuring the ion current resulting from ionization of the ambient gas by the electrons emitted from a heated filament. In normal operation, the ions so created are collected by a negatively biased electrode and the ion current thus measured is proportional to the gas pressure. The gauge can be converted into a usable ion source by appropriate modification of the electrode structure and applied voltages, for extraction of ions from the ionization region to form a beam [15], [16], [17], [18].

Sources of his kind have been made that produce beams of gaseous ions with currents up to microampere at energies of up to several kilo volts. The energy spread of the extracted ion beam in some sources of this kind was found to be a few electron volts and the ions were predominantly singly ionized. Typical operating pressure may be from below 10^{-5} Torr up to about 10^{-3} Torr.

We have used the concept of the sources described above and refined it by designing the geometry of the electrodes using computer simulation of electric fields and ion trajectories rather than relying on the configuration of the commercial gauge. An ion

source designed on the above principle consists of two major parts, the ionizer and an ion extraction and focussing system.

3.2.1 The Ionizer

The ionizer consists of an anode, a cathode and the supporting structure. The cathode is a tungsten filament heated by a current of few amperes. The anode is a cage made up of helically wound tungsten wires. The electrons emitted from the filament are accelerated to the anode (cage) by a potential difference ($V_c - V_f$). Because of the open structure of the cage made of a tungsten wire, a large fraction of the energetic electrons oscillate within the cage where they interact with the gas molecules resulting in the ionization. The electrons are eventually picked up by the positive anode after several oscillations.

The ionizer operates as a thermionic diode which depending on the physical conditions of the diode (anode cathode distance, cathode temperature, accelerating voltage), can operate in two different regimes (or modes).

At a relatively high anode voltage and low filament temperature, the electron density (space charge) near the filament is low. Under those conditions the temperature of the filament controls the electron emission current, which can be described by the Richardson equation [19],[20].

$$J = A.T^2 \, e^{-(e\phi)/(kT)} \quad (1)$$

where: J - Current density

A - Richardson Constant

T - Temperature in deg K

e - Electron Charge

Φ - Work Function

k - Boltzmann Constant

Since the electron current that can be drawn from a filament is limited by its temperature, it is essential to maintain the filament at constant temperature for stable source operation. As the filament temperature increases, the Richardson equation does not follow the emission current. At high temperatures, electrons emitted from the filament are in large enough numbers to produce a space charge around the filament. It is this space charge that limits the amount of electrons which can be emitted, and so limits the emission current. Under these conditions, the thermionic diode is said to be in the space charge limiting mode. The Langmuir-Child equation describes this mode of operation quantitatively [19], [20]·

$$J = B \left(V^{3/2} / d^2 \right) \qquad (2)$$

where: J - Current Density

V - Cathode-Anode Voltage

d - Cathode-Anode Distance

B - Constant = $2.335.\ 10^{-6}$A / unit area

If the diode is operating in the emission limited mode defined by the Richardson equation, the electron current I_e can be varied by adjusting the filament temperature. If the diode is operating in the space charge limiting mode defined by the Langmuir-Child equation, I_e can be varied by adjusting the electron accelerating voltage. If the diode is operating between the two modes of operation, then I_e may be controlled by both filament temperature and acceleration voltage. It should be pointed out that both equations (1) and (2) are valid for a simple one dimensional case and cannot be directly applied to a complex three dimensional geometry of the ionizer described here. Nevertheless the thermionic emission and space charge density limits are preserved also in the complex

three-dimensional case. Thus I_e cannot be effectively defined by either the Langmuir-Child equation or Richardson equation.

3.2.2 Ion Extraction System

The ions created in the ionizer have to be extracted and accelerated to form an ion beam. The process of pulling them out of the ionizer with an electric field is known as extraction. The requirements for extraction are:

- The existence of an aperture in the ionization chamber through which ions can exit.
- The presence of sufficient electric field of appropriate polarity to attract ions out of the chamber.
- Proper shape of the electric field to extract maximum ions with similar velocity and direction.

Extraction is accomplished by an electrostatic field at the exit of the ionization chamber created by applying a potential difference between the ionization chamber and the extraction electrode. The field extends into the ionization chamber and its polarity is such that the chamber is at a higher potential than the extraction electrode. The result is that the extraction electrode attracts the positively charged ions.

The extraction electrode is followed by an acceleration electrode, which is more negative than the extraction electrode. This potential drop (usually a few kV) accelerates the beam. The accelerated ions may then be focussed using a set of electrodes, which shape the beam and focus it at a desired distance.

The extracted beam is influenced by a number of factors including the applied field strength, the shape of the electrodes and the distance between them and the space charge density of the resulting beam itself. It is assumed that in the case of the experimental ion source the space charge density of the extracted beam is low and can be neglected.

We have a used an ion optics program SIMION (Version 6.0) to design the electrode geometry, and to determine their potentials for effective extraction and focussing of the beam.

3.3 Simulation of the Electron Impact Source using SIMION

SIMION is a PC based ion optics simulation program that models ion optics problems with 2D symmetrical or 3D asymmetrical electrostatic or magnetic potentials. It incorporates a so called *"ion optics workbench"* that allows sizing, orientation and positioning of up to 200 instances (2D or 3D images) of *"potential arrays"* within the workbench space. The *workbench* consists of up to 10^6 points (elements) and its volume can be scaled up to 8 km^3. Complex systems or even entire instruments can be modeled. Ions can be flown in singly or in groups, displayed as lines or dots, and automatically be *"re-flown"* to create movie effects. Other features include data recording, charge repulsion, user programs and geometry files [13].

SIMION makes use of *potential arrays* that define the geometry and potentials of the electrodes and magnetic poles. The potentials of points outside electrodes and poles are determined by solving the Laplace equation by finite difference methods. This is called refining the array. Refined array can then be projected as instances into an ion

optics workbench volume. Ions can be flown within the workbench volume and their trajectories are determined by the fields of the potential array instances they fly through. The program does not account directly for the space charge of the ions.

A typical simulation in SIMION consists of the following steps.

- A potential array of the required size (100 x 20, 100 x 500 etc...) has to be chosen along with the type of geometry for the objects to be drawn (planar or cylindrical). The maximum size of the array is 1000000 (100x, 100y, 100z).
- Objects have to be drawn in the *potential array*, each object has to be numbered and its type specified (electrode or non-electrode). Arbitrary potentials are assigned to the electrodes at this stage. (eg. 1V, 2V, 3V... etc)
- When the entire drawing is complete, the *potential array* has to be *refined*. Refining takes time, the 300 Mhz Pentium P2 processor, 64 MB RAM PC which was used in all of our simulations took about 4 minutes to refine a potential array with 7 electrodes in a 2.10^5 element optical *workbench*.
- Once the array has been refined, the potentials have to be set on the electrodes. This is called *"Fast Adjusting"*. Now ions can be defined (number of ions, starting point, single or grouped etc). Once defined, ions can be flown and the trajectories can be observed. This process is fast and takes few seconds in this case.

We have used a 1000 x 200 2D array with cylindrical geometry for all the models i.e. 1000 points on the X-axis and 100 on the Y-axis. The distance between adjacent points in the array corresponds to a millimeter and a scale of 1:4 was used when drawing objects.

One of the main design considerations when simulating the ion source model was to focus the beam at a spot 10.5 inches (~ 27mm) from the analyzer magnet. This point is

seen as an object by the magnet, which then focuses it at an image distance. So, the objective of the ion extraction and focussing systems was to focus the beam at this point and has been considered in the simulations.

3.3.1 Preliminary Design

The ionizer along with a set of extraction & focussing electrodes was modeled as in Fig 3.2.

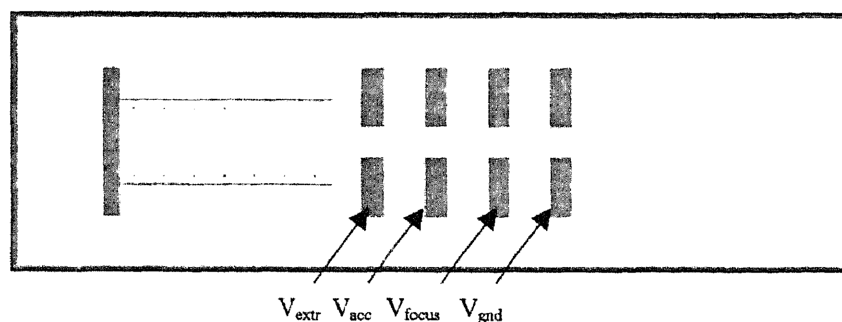

Fig 3.2 Preliminary design of the ion source

The source along with its housing is seen in the 2D view above. The anode (seen as series of dots) is 2'' long and 0.1''in diameter and the filament is at a distance .1'' from it. All the electrodes were modeled as circular metal rings with an aperture of 0.6'' at the center. Simulations were carried out with this configuration for different sets of electrode voltages with the objective of focussing the beam at the object distance of the magnet. (Fig 3.3).

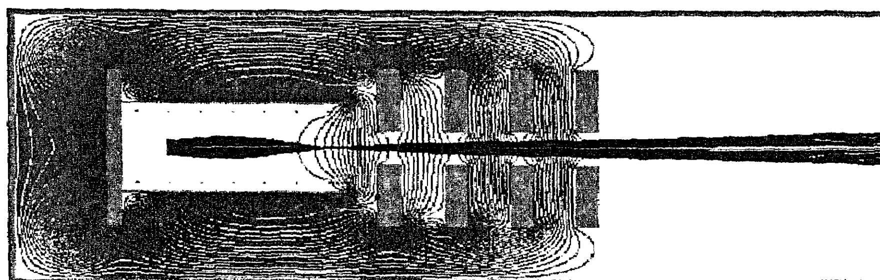

V_{extr} = 1500V V_{acc}=2000V V_{focus}=4000V V_{gnd}= 0V

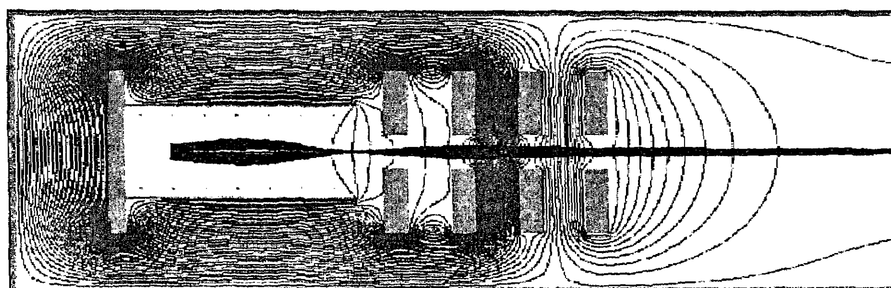

V_{extr} = 1500V V_{acc}=3500V V_{focus}=5000V V_{gnd}= 0V

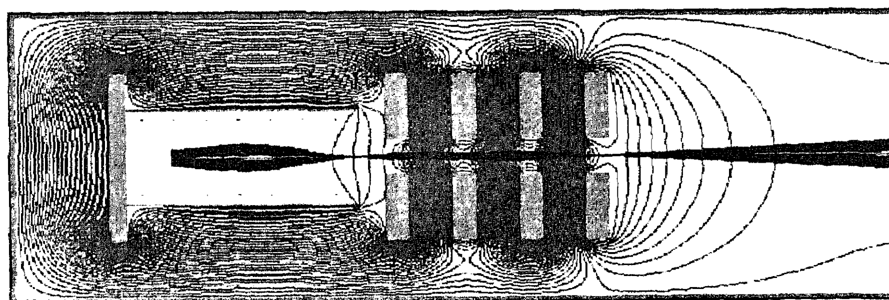

V_{extr} = 1500V V_{acc}=6500V V_{focus}=9000V V_{gnd}= 0V

Fig 3.4 Beam focussing under different electrode potentials

The simulations led to the following observations:

- The field between the grounded enclosure and the electrodes seemed to influence the shape of the beam.
- It was observed during simulations that the beam could be extracted and focussed using three electrodes instead of the four i.e. an extraction electrode followed by an accelerating electrode and a ground electrode would be sufficient for focussing.
- It was also observed that ions generated farther away from the extraction electrode were not being extracted. Instead, these ions traveled in the opposite direction to the beam, as shown in fig 3.5

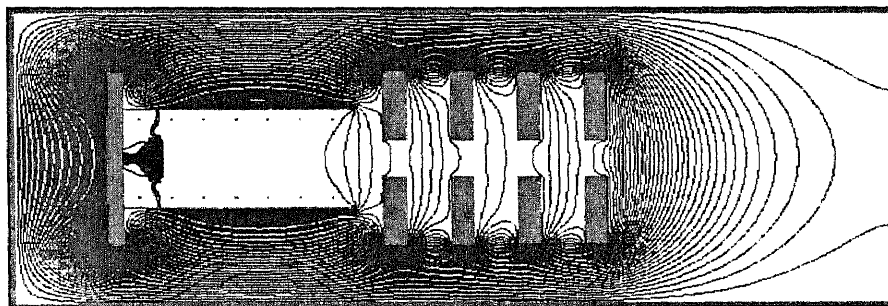

Fig 3.5 Ions generated farther from the extraction electrode unable to be extracted

Next, simulations were carried with different sets of voltages on the electrodes (with the view of eliminating the lens electrode). The anode structure was modified to attract ions generated farther away from the extractor. A refined version of this design was developed and is shown below.

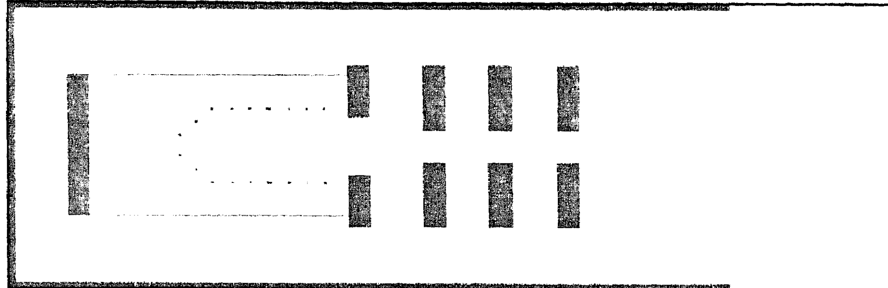

Fig 3.6 Modified version

3.3.2 Modifications

The bottom end of the cage was cone shaped to prevent ions from travelling in the opposite direction to the beam. The length of the cage and the distance from the extractor was shortened for the extraction field contours to reach far inside the cage. A shield held at the filament potential was placed just in front of the cage to prevent ions from escaping from the ionization region. Also, the possibility of beam extraction and focussing using a set of 3 electrodes was explored.

It was found that these modifications yielded better results compared to the earlier version. The beam focussing however was still very strongly dependent on the portion inside the cage where the ion trajectories originated i.e. the focussing condition for ions starting at somewhere in the middle of the cage, was very much different for ions which originated either close/ far from the extractor.

3.3.3 Final Design

The above problem was overcome with a modified design based on an ion source developed by J.Kirschner [16]. This modified source model along the beam focussing under different conditions is shown in Figs 3.7 and 3.8 respectively.

Some of the salient features of this design were:

- This design was characterized by long tubular electrodes inside which the field is relatively weak. By contrast high fields existed in the gap between electrodes in the earlier designs.
- The extractor extends to the opening of the cage in this design and is very different from the earlier designs. By having such a configuration, extraction field contours penetrated much deeper inside the cage, thereby extracting more ions.
- The equipotential contours near the extractor are concave so that the ions, mainly generated off axis, are radially accelerated towards the axis. The divergence of the beam is reduced by the lens action of the accelerating field between the extractor and accelerator.
- Simulations carried out using this model showed different focussing characteristics. It was far easier to focus the beam in this design and the focussing spot could be adjusted with small changes in extraction and acceleration electrodes.

This model formed the basis for the construction of the ion source.

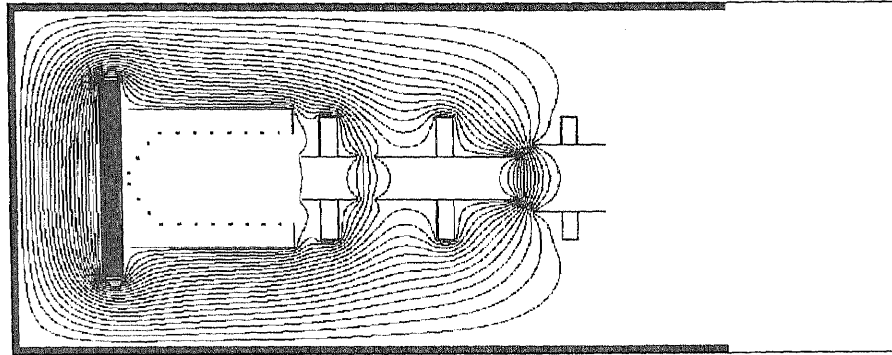

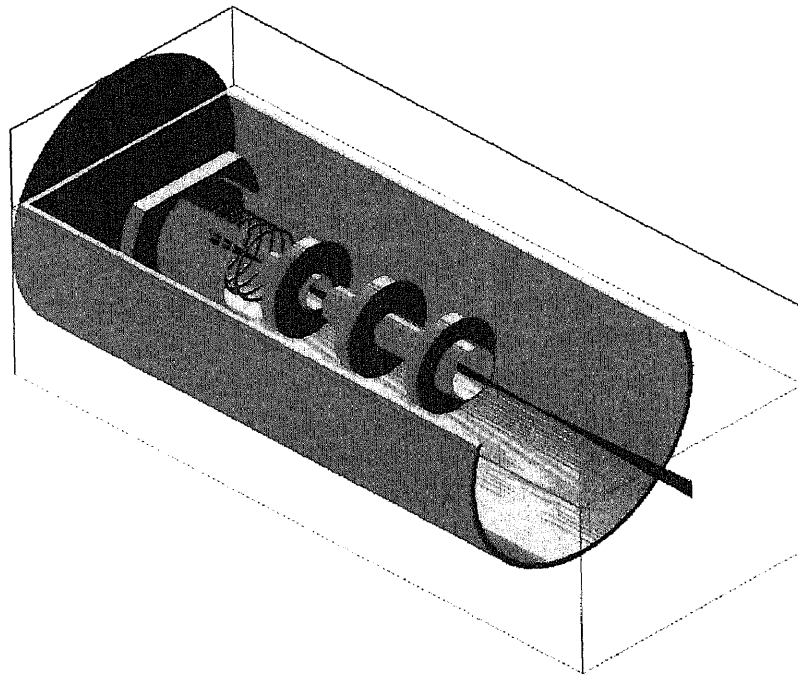

Fig 3.7 The Final Version of the Source in 2D and 3D views

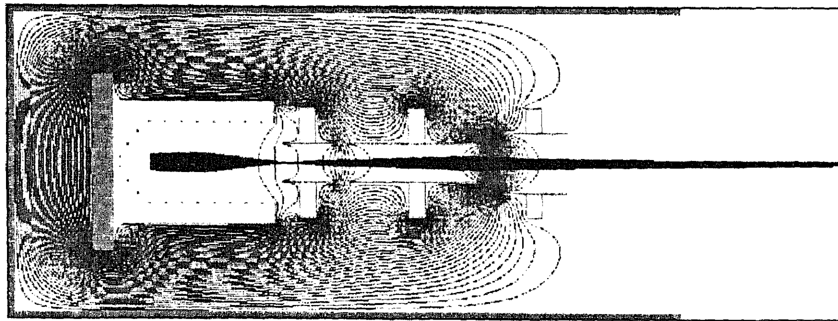

(a)

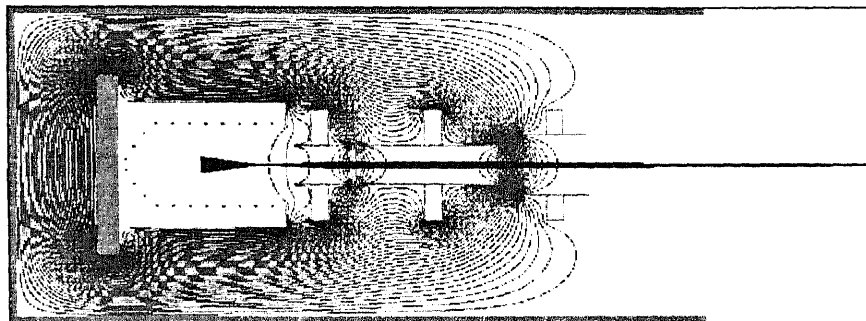

(b)

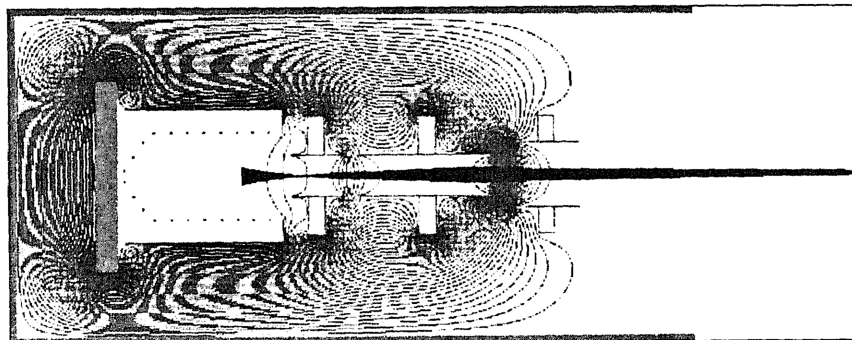

(c)

Fig 3.8 Beam focussing at various starting locations

Fig 3.8 shows focussing of ions that originate close to the bottom of the cage, center of the cage and region close to the extractor. The beam could be focussed easily with small changes in electrode potentials.

3.3.4 Summary of Simulation Results

Simulations provided us with valuable information on the effect of ionizer geometry, electrode configuration and the voltages required for extraction and focussing of the ion beam. Typical focussing conditions at various acceleration voltages are shown Table 3.1. These conditions helped us to determine the power supplies required for the extraction and focussing electrode.

Table 3.1 Summary of simulation results

h.v. Acceleration Voltage	Extraction Voltage	Focussing Voltage
20kV	750	5000
	1000	7000
10kV	250	2500
	500	4000
	750	6000
5kV	250	1500
	500	4000
	750	6000
3kV	250	950
	500	2850
	750	6500
2kV	250	580
	500	1050
	750	5500
1kV	250	260
	500	300
	750	3500

3.4 Description of the Ion Source Structure

The ion source model discussed in the previous section could be translated into a physical structure in a number of ways. One important consideration while constructing the source was the availability of a 20 kV high voltage bushing from an Eaton 3200 implanter. This high voltage bushing provided two advantages.

- It isolated the source and sub system operating at 20 kV from the rest of the beamline, thereby the entire system except the source could be at ground potential during operation.
- Since it was a standard bushing used in a commercial implanter, the ion source supported by this bushing could easily be transported for use on the implanter in future work.

The ion beamline structure supporting the experimental ion source is shown in Fig 3.9

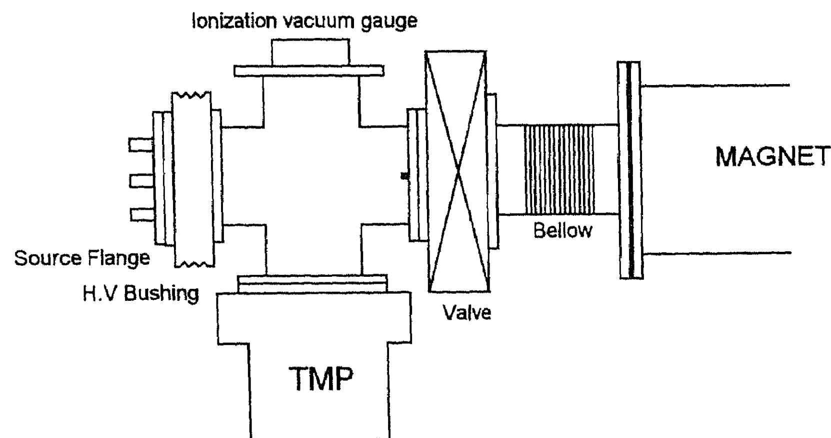

Fig 3.9 Source end of the beamline

Dependex flange system was used to build the beamline and a dependex 4"x 4"way cross was used for housing the source structure. As seen in the figure, the source system consisted of a source flange (which held the entire ionizer and electrode assembly), the h.v bushing, the 4"x 4"stainless steel cross and a valve leading to the magnet. Transition flanges were designed and machined to attach components between standard dependex and the magnet chamber.

3.4.1 The Source Flange

On a standard 4" dependex stainless steel flange, ten electrical feedthroughs (Part No EFT 1212251 Kurt J Lesker Co) were welded on a 2.75" diameter circle. These feedthroughs of standard UHV metal ceramic type were rated for 12kV, 7A. Even with the source flange grounded, and without the h.v bushing, the source could be operated upto 12kV. The source flange prior to the source mounting is shown in Fig 3.10

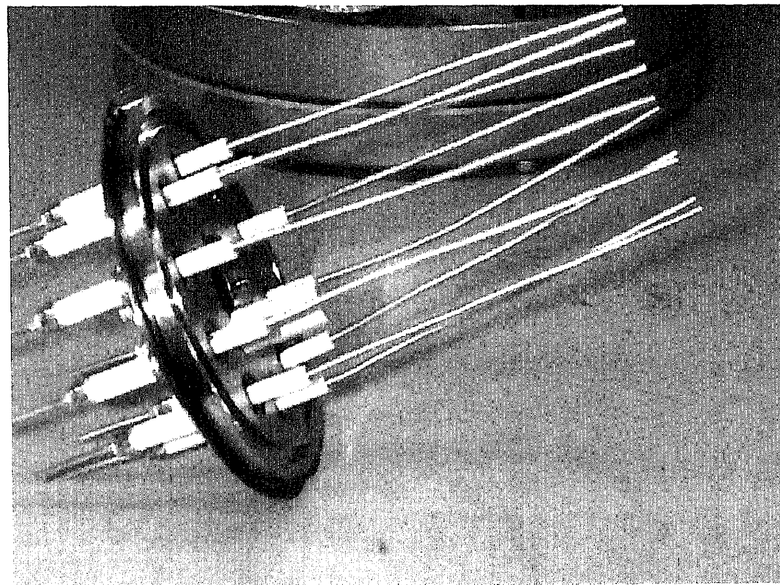

Fig 3.10 The Source flange

At the center of the flange, an $1^1/_3$"conflat flange was welded for gas feed. On the inner side of the source flange, three holes were threaded (8-32) on 1.2" dia for holding ceramic insulators which supported the entire source structure

3.4.2 The Ionizer

The structure was constructed entirely from eV parts supplied by Kimball Physics Inc [21]. eV parts are an assortment of several hundred standard components made of stainless steel, refractory metals and high purity insulators, designed specially for high vacuum environments. The utilization of eV parts had two advantages, first, it eliminated the need to machine many components and second, there was a readily available supply of replacement parts if need arose.

The source base was a 2" dia, 0.6" thick aluminum plate supported by three insulators screwed to the source flange. The ionizer structure is seen in Fig 3.11. The structure was supported by 3 metal rods 1.5" long and .185" dia. holding a pair of eV plates on either side. The set of plates facing the electrode assembly was of ¾" diameter and the set at the other end was of ½" dia. Ceramic tubes ¼" long, 0.125" dia were used to isolate the filament and cage leads from the ionizer structure.

The anode was made up of tungsten wire 0.0.15"-dia wound in the form of a cage of 5 turns. It was connected to one of the electrical feedthroughs by a copper wire.

The filament was made up of 0.005"-dia-tungsten wire and held by tantalum supports made up of 0.5mm wire. The distance of the filament from the cage could be adjusted by bending the tantalum supports.

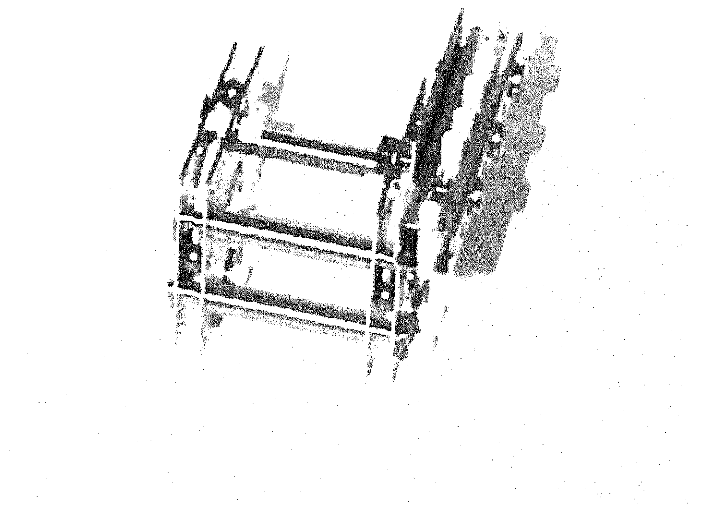

Fig 3.11 The Ionizer structure

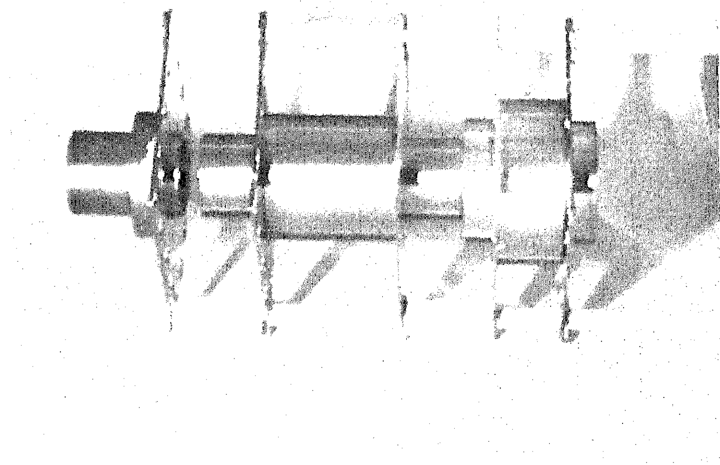

Fig 3.12 The Electrode assembly

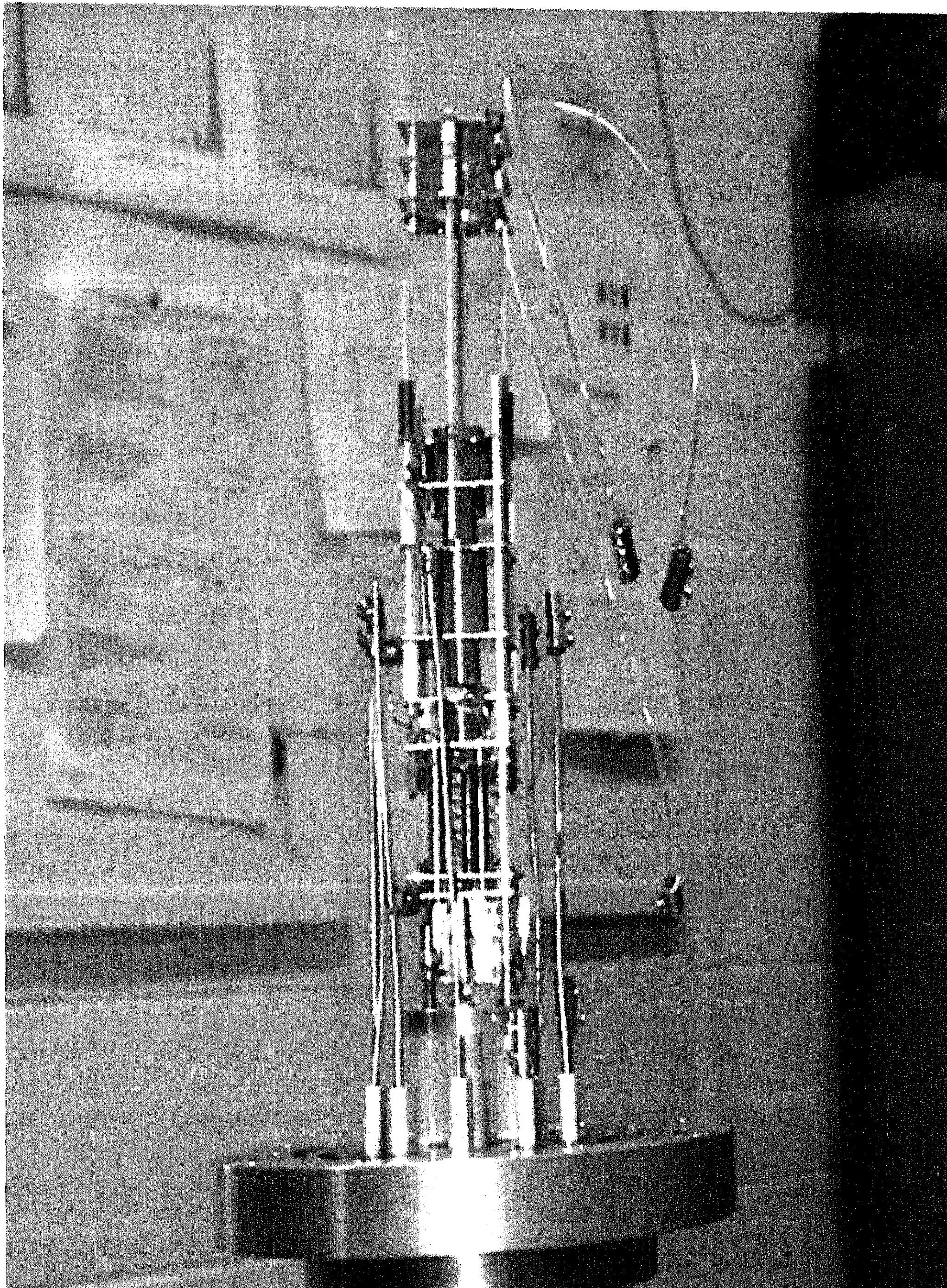

Fig 3.13 The Ion source

3.4.4 Electrical System for the Ion Source

The wiring diagram for the ion source is shown in Fig 3.14.

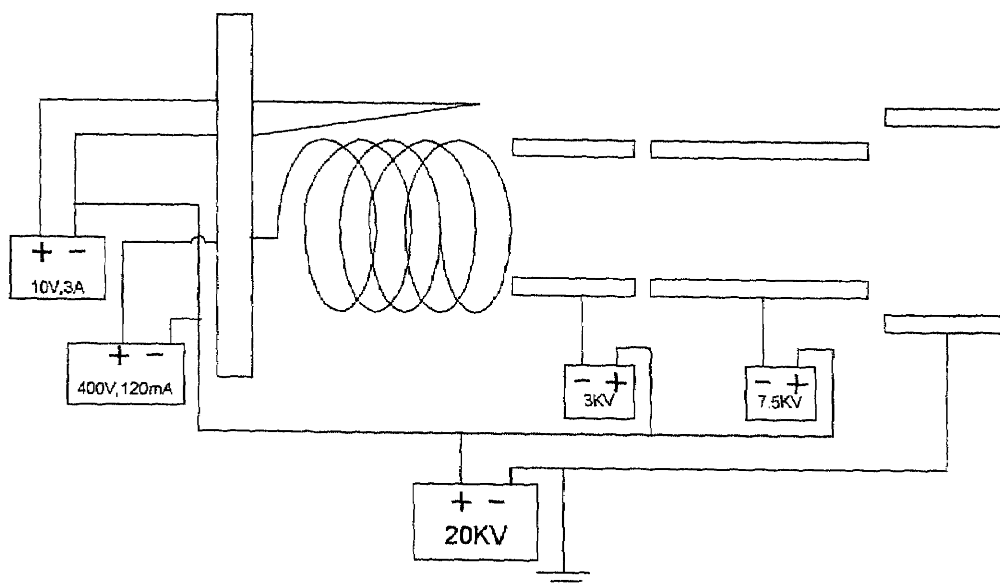

Fig 3.14 Schematic of the electrical connections

The filament was supplied by a (0-10V), 5A DC Power Supply and a (0-400V), (0-120mA) DC power supply (hp, Model 6209B) powered the anode.

For the extraction and focussing electrodes, power supply modules operating on 15V DC were used. A (0-3kV), 1mA module (Bertan, Model No PMT-30C/1V) supplied the extraction electrode and a (0-7.5)kV, 250μA (Bertan, Model No PMT-75C N-S). A 20kV isolation transformer was used to supply power to all the source power supplies.

All the source power supplies were mounted on a shelf and isolated from the rest including body of the shelf. The output of the 20kV, 120mA high voltage power supply (cps Inc) was connected to the source power supply shelf.

CHAPTER 4

MEASUREMENT OF CHARACTERISTICS OF THE ION SOURCE

In this chapter, the procedures and results of the experiments conducted to investigate the operational characteristics of the new source are discussed.

4.1 Ionizer Filament Emission Characteristics

This experiment determined the emission characteristics of the ionizer filament.

- *Experimental procedure*

With the anode (cage) voltage V_c set to 0V, the filament heating current was increased from 1.5A to 3.5A in 0.25A increments. At each filament current setting the filament potential was varied from 0V to -280V in 20 V increments. At each voltage and heating current setting, the filament emission current was measured and recorded. The pressure in the chamber was 1.3 x 10^{-5} Torr.

- *Experimental Results*

The results of the experiment are summarized in table 4.1 and figure 4.1. The ionizer characteristic curves indicate the relationship between the filament heating current (I_f), accelerating voltage and the resultant filament electron emission current. With a filament heating current of 2A and accelerating voltage greater than about 60V, the ionizer operates in the emission limited mode. At a filament heating current of 2.25A the characteristic is clearly space charge limited up to about filament voltageV_f=150V where the emission limit begins. At V_f=100V which is of interest for decaborane ionization the

filament operates in the transition range; electron emission current increases with the filament current from 25mA at I_f=2.25A to 3.2mA at I_f=3A.

Table 4.1 Ionizer filament emission characteristics with the first version of the ionizer

IONIZER FILAMENT EMISSION CHARACTERISTICS							
Filament current If							
	1.5A	2A	2.25A	2.5A	2.75A	2.85A	3A
Vf		Electron Emission Current (Ie) in mA					
0	0	0	0	0	0	0	0
20	0	1	1.5	1	1	1.1	3.2
40	0	3.75	5	5	5	5.2	8
60	0	5	10	10.5	11	10.8	15
80	0	5.5	20	20	20	20	22
100	0	5.5	25	26	28	28	32
120	0	5.8	32	34	38	38	45
140	0	4	40	45	48	45	58
160	0	4	48	55	58	55	75
180	0	7	50	68	71	70	
200	0	8	51	75	76	75	
220	0	8	55				
240	0	9	60				
280	0	10	60				
320	0		60				

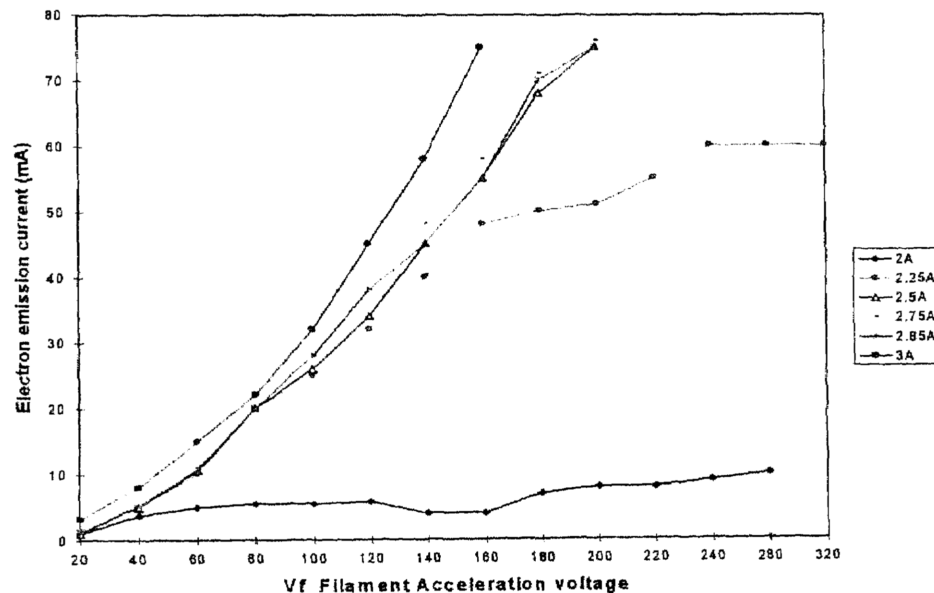

Fig 4.1 Ionizer filament emission characteristics

4.1.1 Problems Faced during Initial Ionizer Operation and their Solutions

One of the main problems faced during operation of the first version of the ionizer (whose characteristics were explained in the previous section) was the frequent burn out of the filament. This filament was held by two tantalum supports at its opposite ends and possible reasons for the frequent filament burn out could be attributed to a large power dissipation over the short length of the filament wire and kinks on the filament incurred when inserting it to its final position.

To solve this problem, the filament length was extended and an additional support was added in its middle. The modified filament was V shaped, (almost twice the length of the earlier one). Two tantalum wires supported it from the top end and another support at the bottom. Care was taken not to form any kinks on the filament while inserting it into position.

The modified shape of the filament proved to be more stable and the filament life was considerably longer. However, there was not much of a difference in the filament emission current although the length of this filament was twice the length of earlier one. The ionizer was further refined by adding one more V shaped filament on the opposite side of the cage. Two filaments provided the following possibilities:

- The extra filament could be used without removing the source in case the first filament burned out.
- The two filaments could be connected in series to explore the possibility of obtaining more electron current.

With this new structure, filament emission characteristics were measured with the following configurations.

a) With Filament1 only. (Table 4.2, Fig 4.2)

b) With Filament2 only. (Table 4.3, Fig 4.3)

c) Filament1 and 2 connected in series. (Table 4.4, Fig 4.4)

Some of the observations from these measurements were as follows:

- Each filament provided different electron currents. At V_f=100V and I_f=2.25A, electron emission current using filament1 was 20.3mA, and 11.5mA with filament2.
- When connected in series, we realized an electron current of 31.4mA, which is approximately the sum of the electron currents obtained from each individual filament. Thus more electron current could be realized by using two filaments in series.
- With the two filaments in series, it was not possible to achieve filament currents greater than 2.4A. with the available power supply. Higher filament current, however did not result in appreciable increase in electron current in the potential range of interest for decaborane ionization (70-80 eV).
- The filament operation was stable, even at extended periods of operation.
- It is possible to achieve greater electron currents at higher V_f (2-4 times more than at 240V). However this electron current increase is comparable to the decrease of the ion intensity at higher electron energies (see Fig 2.5) and would not be expected to yield higher ion currents from the source.

Table 4.2 Ionizer filament emission characteristics with filament1

	Filament Current If				
Va	**2A**	**2.25A**	**2.5A**	**2.75A**	**3A**
0	0	0	0	0	0
20	1.7	0.9	0.8	0.9	1.1
40	5	5	5.1	4.9	5.4
60	6.6	10	11.6	11.1	11.7
80	7.9	15.3	19.1	18.1	19.5
100	8.3	20.3	27.6	26.2	28
120	9.3	23.9	36.6	35	36.9
140	12.5	25.8	45	44.2	47.3
160	10.3	26.4	54.5	54.2	57.3
180	15	26.7	61.8	62.5	63.1
200	5	26.9			
220	5	26.1			
240		25			

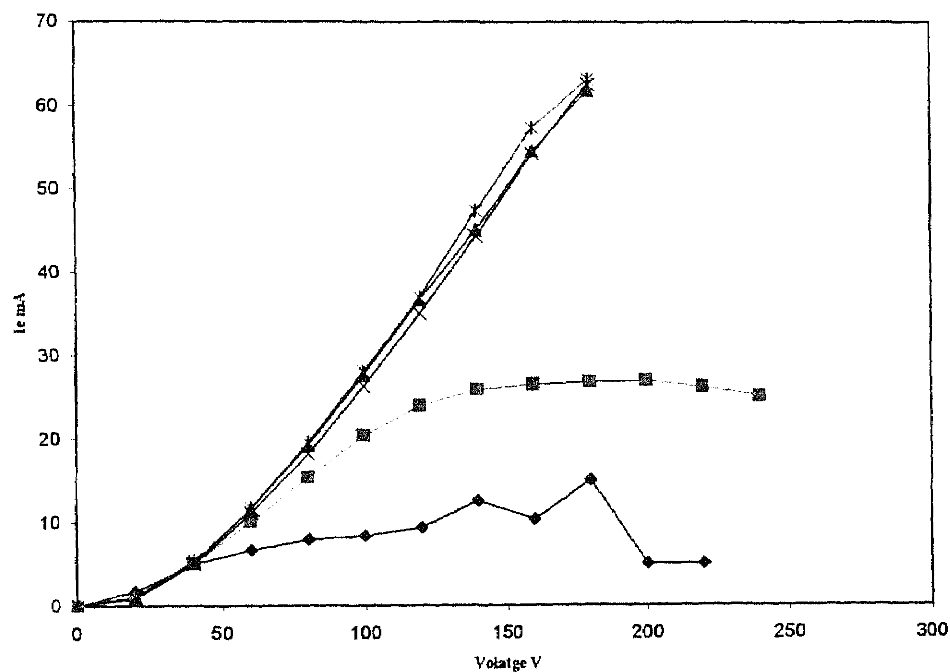

Fig 4.2 Ionizer filament emission characteristics with filament 1

Table 4.3 Ionizer filament emission characteristics with filament 2

	Filament Current If				
Va	2A	2.25A	2.5A	2.75A	3A
0	0	0	0	0	0
20	0.8	0.8	0.7	0.7	0.7
40	2.8	2.8	2.8	2.9	2.9
60	4.7	5.6	5.6	6	5.7
80	5.6	8.6	9	9.5	9.8
100	4	11.5	12.8	13.3	13.8
120	3.8	14.2	16.6	17.3	18
140	3.5	16.5	20.9	22.1	22.7
160	2.3	18.2	25.1	26.9	27.7
180	2.8	18.5	29.1	31.9	32.9
200	2	20.6	33.9	37.5	38.8
220	2		38	43.5	45.1
240	2		42	49.3	52
260	2		46.6		

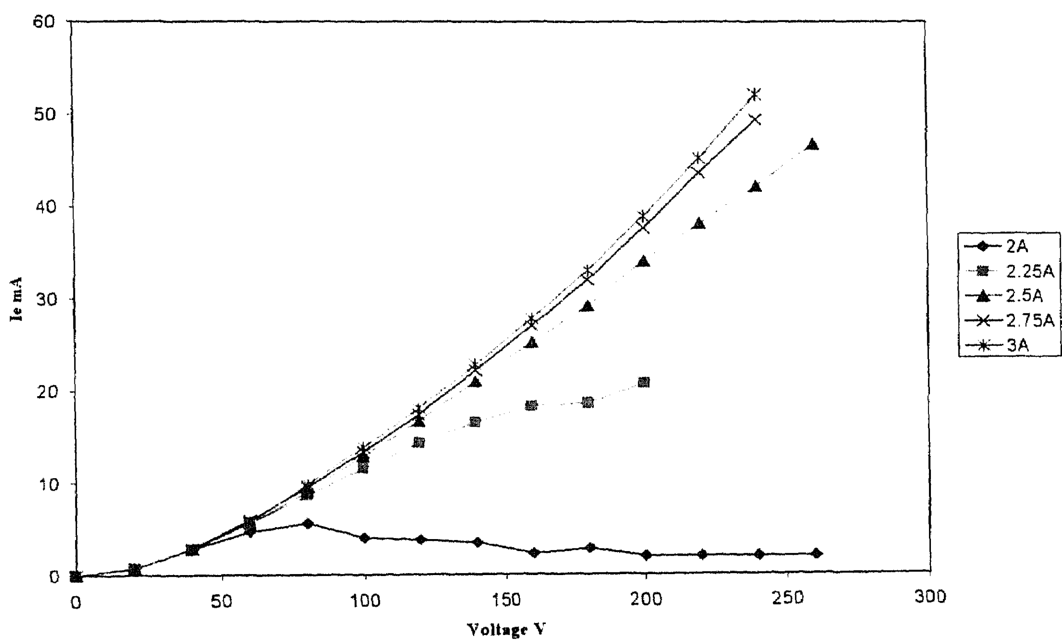

Fig 4.3 Ionizer filament emission characteristics with filament 2

Table 4.4 Ionizer filament emission characteristics with filament 1 and filament 2 in series

	Filament Current If		
Va	2A	2.25A	2.4A
0	0	0	0
20	1.6	2.3	2.2
40	3.2	8.3	8.7
60	4.9	16.1	16.9
80	5.5	23.7	27.4
100	5.1	31.4	33.2
120	5.8	37.8	48.2
140	5.8	42.6	60
160	6.9	42.8	65.1
180	8.5	42.3	
200	9.2	43	
220	10.3	45.8	
240	10.4	50	
260	12.7		

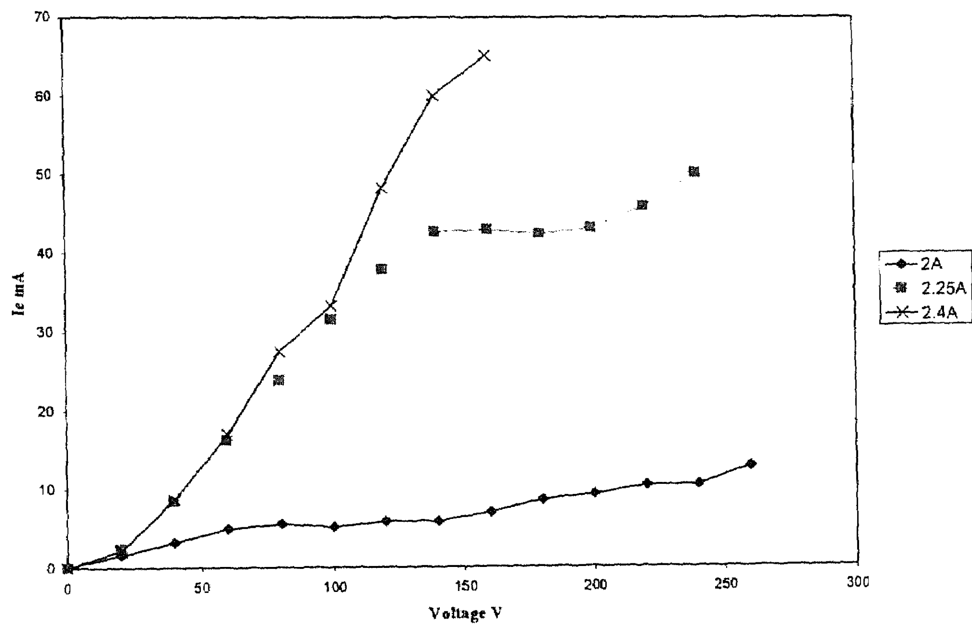

Fig 4.4 Ionizer filament emission characteristics with filament 1 and filament 2 in series

4.2 Ion Current Measurements

The next step after ensuring the stable operation of the ionizer was to test the experimental ion source using an inert gas such as Argon. In this section, the experiments performed to verify ion source operation and resultant ion current measurements are described.

- *Experiment*

Argon gas was admitted to the source gas inlet through a leak valve. In order to observe the ion beam, a phosphor screen was placed at the focussing distance inside the source chamber. The screen could e observed through a view port. A copper wire was attached to this screen and connected to a Pico-ammeter (Kiethley Model No 6904B) through a BNC connector.

The system was pumped to 8.10^{-6}T and the filament current set to 3A. The electron current in the cage was adjusted to 25mA. Argon gas was let in to the source until the source pressure read 2.10^{-4}T. The source was then placed at 2kV by using the 20kV high voltage supply. At this accelerating voltage, the potentials on the extraction and focussing electrodes were varied to obtain focussing. However, the glow inside the source chamber due to the ionizer filament incandescence was so high that it was impossible to observe the ion beam on the phosphor screen. Therefore the beam-focussing conditions could not be measured with this configuration. The accelerating voltage was varied and the maximum ion current attained at each accelerating voltage was recorded as shown in Table 4.5

Table 4.5 Preliminary ion current data

Accel Voltage	Extr Voltage	Focussing Voltage	Ion Current
2kV	500V	1800V	5.9uA
3kV	500V	3500V	4.4uA
5kV	500V	4850V	1.9uA

4.2.1 Ion Current Measurements Using Concentric Apertures

As explained in the previous section, the beam focussing conditions could not be observed with the phosphor screen. Fig 4.6 shows a modified arrangement to determine the focussing conditions of the beam.

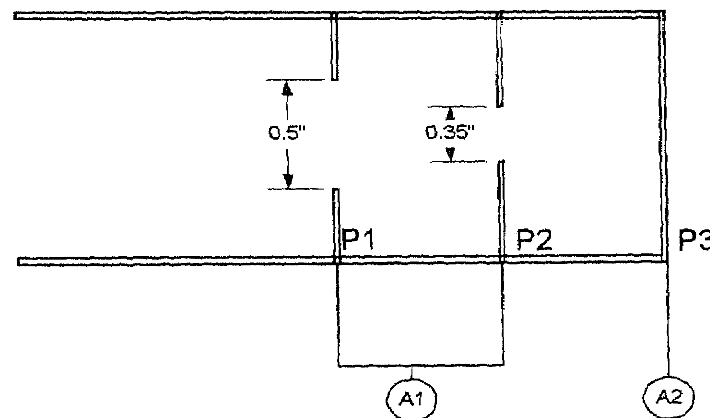

Fig 4.6 Ion current measurements using concentric apertures

A set of 3 plates (eV parts) P1,P2 and P3 were mounted on a ceramic tube(as shown in Fig4.6) and aligned with the source structure such that the blank plate P3 was at the focussing distance of the source (10.5"from the source flange). P1 and P2 were shorted

and connected to a Pico ammeter (A1) and P3 was connected to another Pico ammeter (A2). Using this arrangement, the focussing condition of the beam could be determined when A2 read maximum current and A1 read minimum current.

Table 4.6 summarizes beam focussing under varying conditions. In the table, the maximum current obtained at plate P3 under different extraction and focussing conditions is shown in the second row of each reading.

Table 4.6 Ion current measurements using concentric apertures

Acceleration Voltage	V_{extr}	V_{focus}	Ion Current P1 & P2	Ion Current P3	Remarks
1kV	200	260	67nA	.48uA	Focussed
	200	1000	2.3uA	1uA	
	300	240	12nA	.48uA	Focussed
	300	1310	1.2uA	1.06uA	
	400	250	17nA	.59uA	Focussed
	400	1800	1.13uA	1.14uA	
2kV	200	580	57nA	1.05uA	Focussed
	200	750	.41uA	1.52uA	
	300	550	16nA	.65uA	Focussed
	300	1250	.64uA	1.27uA	
	400	640	45nA	.58uA	Focussed
	400	1400	.63uA	1uA	

4.3 Simulation vs. Experimental Results

The focussing conditions observed during actual source operation were in agreement with the simulations. Consider one of the observations from Table 4.6.

At 2kV acceleration, with an extraction voltage of 200V and focussing voltage of 580V, the beam was well focussed (experimental data). Fig 4.7a shows beam focussing under the same conditions from SIMION.

As the focussing voltage was increased, the ion current increased and the maximum current was attained at 750V. For further increase in focussing voltage, there was a decline in the ion current. Fig 4.7b shows the simulation condition for maximum beam current (not focussed) and Fig 4.7c shows a decline in the ion current for focussing voltage > 750V.

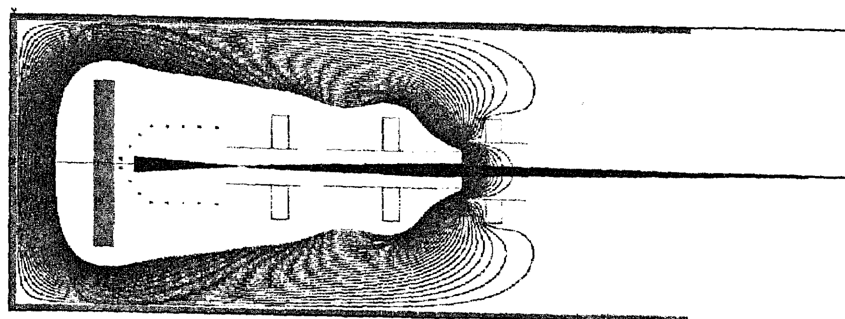

a) Focussing Condition $V_e = 200V$, $V_f = 1420V$

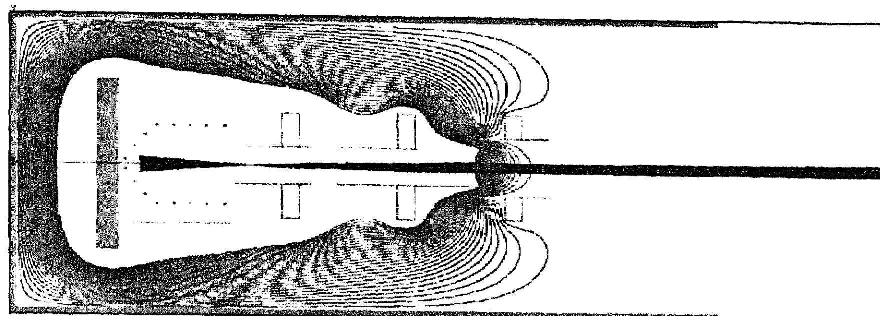

b) Maximum Ion Current at $V_e = 200V$, $V_f = 750V$

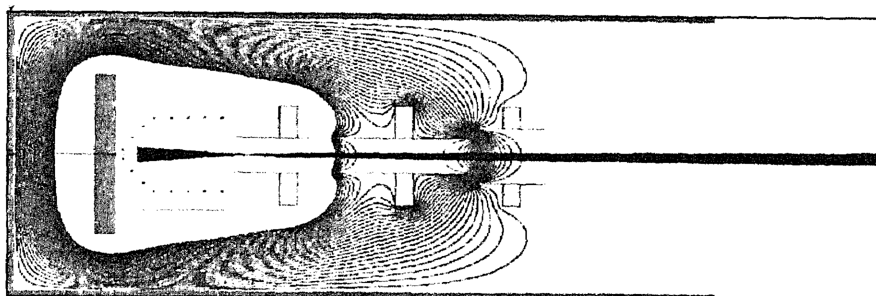

c) Reduction in Ion current for $V_f > 750V$

Fig 4.7 Simulations vs. Experimental data

CHAPTER 5

MASS SEPARATION AND ION BEAM TRANSPORT SYSTEM

Once the ion beam has been generated, it has to be mass analyzed for selecting the ion species of interest according to their mass, focussed at a particular distance and scanned uniformly over the target. In this chapter, the 20keV-research implantation system currently being developed at NJIT is described.

A schematic of the ion implantation system is shown in Fig 5.1. It is comprised of four main sections:

- The Ion Source
- The Magnet
- The Beamline
- The Sample Chamber.

The ion source has been described in Chapter3. The magnet, beamline and the sample chamber will be briefly discussed in this chapter.

The entire beamline is being built using 4" Dependex type vacuum parts and spans approximately 6ft. The source along with its power supplies is at high voltage and the rest of the beam line including the target chamber is at ground. The source end of the beamline connects to the magnet entrance through a bellow. Bellows are flexible elements in the beamline and provide small adjustments in beamline direction and height. Transition flanges were designed and machined to connect the magnet to the dependex flanges of the rest of the system.

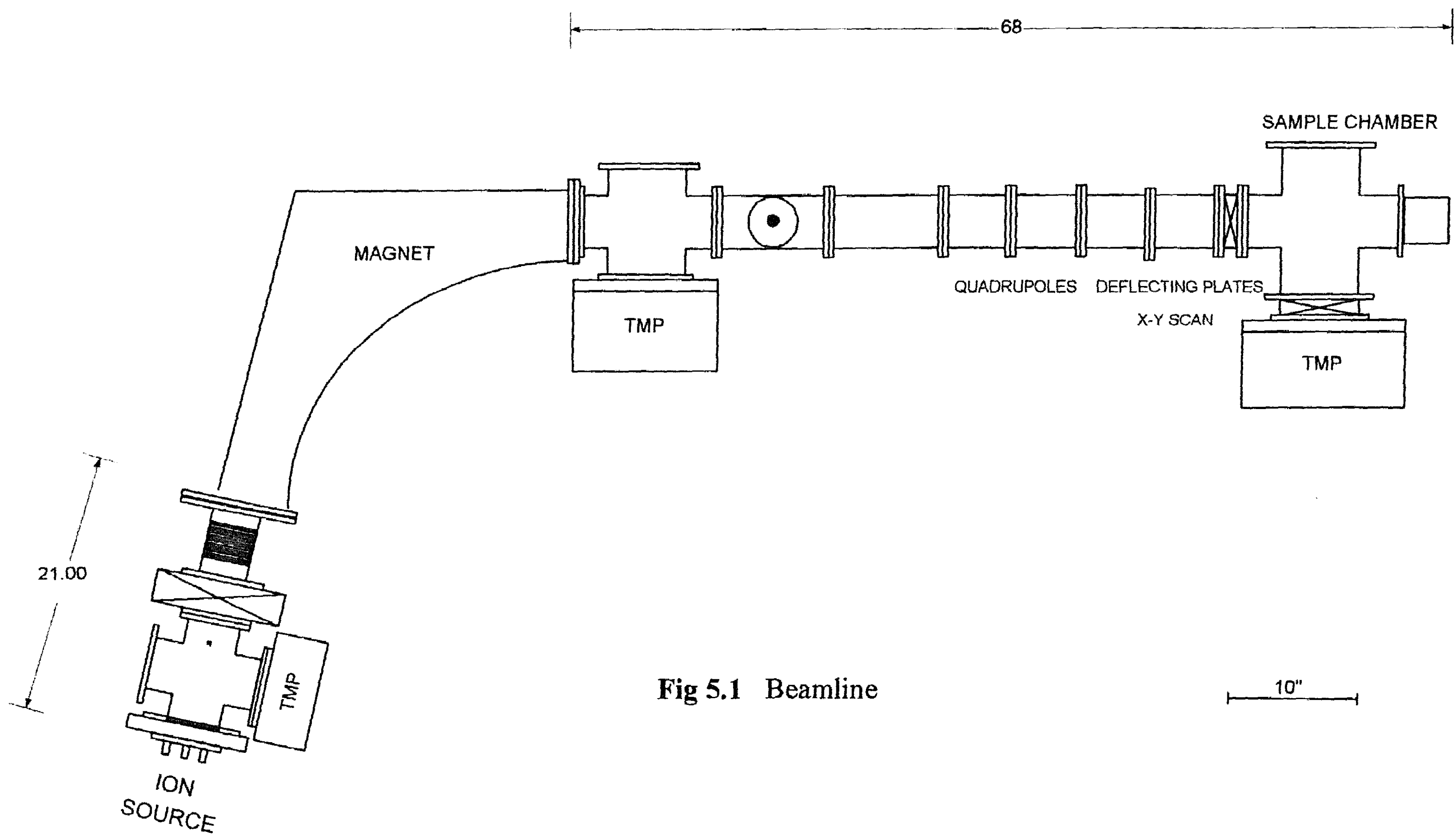

Fig 5.1 Beamline

- **The Magnet**

A mass analyzing magnet positioned along the beam path between the source and the process chamber filters ions from the beam while allowing certain other ions to enter the process chamber. The magnet includes multiple magnet pole pieces constructed from a ferromagnetic material and having inwardly facing pole surfaces.

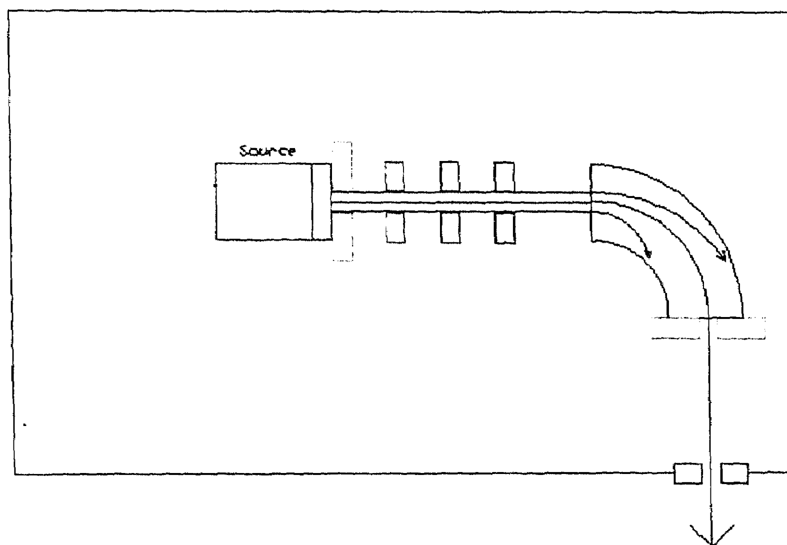

Fig 5.2 Illustration of the analyzer magnet operation

As the ions travel through the magnetic field, the magnetic force serves to move them in a circular path, according to the right hand rule. Heavier ions strike the outer wall, lighter ions strike the inner wall, only ions of specific mass-charge ratio pass through. The mass resolution is further enhanced by an adjustable exit aperture positioned at the focal point of the magnet on the exit side. The formula for the radius of curvature.of the ion trajectory in the magnet is given by

$$R = (1/Bq)(2mE)^{1/2} \quad (3)$$

where: R is the radius of curvature of ion path in cm

B is the magnetic field in kilogauss

m is the mass of the ion

E is the ion energy in keV

q is the charge state of the ion (1,2 ......)

A 70°-analyzer magnet from an Eaton Implanter is being utilized for mass analysis. Ions that follow the trajectory with radius R are deflected through the 70° sector of the magnet and brought to a focus in the resolving slit located at a distance 14.5" from the magnet exit.

- **The Beamline**

The beamline consists of the following components:

- *Resolving Aperture*

The resolving aperture or slit is used to improve beam resolution and adjust the beam current. The slit can be controlled manually.

- *Quadrupole Assembly*

After the beam passes through the resolving aperture, it enters the electrostatic quadrupole lens assembly. A quadrupole consists of 4 poles with polarities as shown in the Fig 5.3. By applying voltages with appropriate polarities on these poles, the beam can be focussed into a desired shape and size.

We have used a pair of quadrupoles with the following specifications.

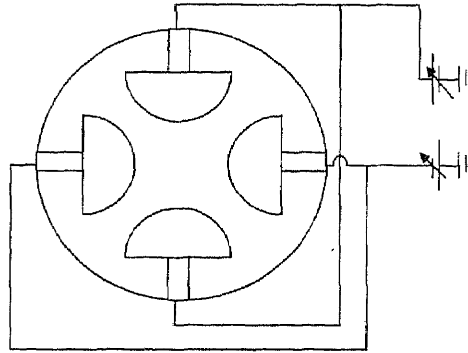

Fig 5.3 Quadrupole

Pole length - 3.8"

Gap between X and Y elements - 2"

Pole Separation - 0.9"

Pole Radius - 1"

- *Deflection Plates*

The beam then passes between horizontal and vertical scan plates that cause the beam to scan across the target. We have used scanning plates with the following dimensions

Plate length - 3.8"

Plate Width – 1.5"

Distance between the plates - 1.5"

- **Sample Chamber**

The target chamber holds the sample to be implanted along with the ion current measuring devices (Faraday Cup). A beam line valve (BLV) separates the target chamber from the rest of the system. The target chamber is pumped separately and with the BLV closed, wafers could be removed / inserted without venting the entire system.

CHAPTER 6

CONCLUSIONS

From the study of ionization of decaborane by ion mass spectroscopy for electron impact energies from 20eV to 255eV and temperatures up to 350^{0}C, we arrived at the following conclusions.

- The decaborane molecule was found to be more robust than expected.
- The abundance of ions containing 10 B atoms ($B_{10}H_x$) has a maximum at $E_e \sim 70$eV.
- Ions containing 10 B atoms dominate the mass spectra and contribute to ~ 80% of the ion current.
- The abundance of $B_{10}H_x$ ions does not vary appreciably on temperature upto 350^{0}C.

Preliminary data on the operational characteristics of the experimental ion source indicate that Ar^+ beams of several microamperes can be achieved. Also, there is qualitative agreement between beam focussing conditions and simulations. The source will be a part of the experimental ion implantation system being built at the Ion Beam and Thin Film Research Laboratory at NJIT.

APPENDIX A

DECABORANE

Decaborane is the largest and the most stable among the hydrides. In this section, general information regarding the structure, physical and chemical properties of decaborane and most importantly the safety aspects to be taken care of while handling decaborane are described.

- **Structure, physical and chemical properties**

Decaborane molecule comprises a cage of ten Boron atoms in which each boron atom is bonded normally to one hydrogen atom, the remaining four hydrogen atoms forming single-atom bridges between four pairs of ten boron atoms. Most of the boron-boron bonds in the compound do not involve any hydrogen bridging. The average boron-boron bond distance in the molecule is 1.77 A.U but each boron atom forms part bonds at various distances with its boron atom neighbors [22].

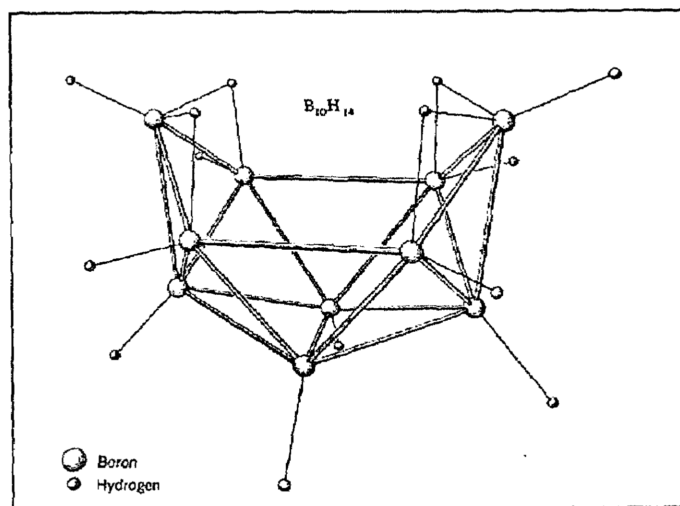

Fig A1 Structure of the decaborane molecule

Formula	$B_{10}H_{14}$
Molecular Weight	122.31
Description of Substance	Colorless to white crystalline solid with an intense, bitter, chocolate-like odor.
Melting Point	99.7° C
Boiling Point	213° C
Density	0.94g/cc at 20°C
Vapor Pressure	19 mm Torr at 100°C.
Heat of Sublimation	19.4 kcal/mol.

The most stable of the known Boron hydrides, decaborane is stable indefinitely at room temperature. In absence of air, it can be heated to 150°C for extended periods without decomposition. It decomposes only slightly in 48 hrs at 200°C.Decomposition to hydrogen and a solid composition $B_nH_{0.6n}$ is complete in 25 hrs at 250°C, but decomposition into boron and hydrogen is very slow at 300°C.

- **Material handling and safety**

Decaborane can be stored in any weatherproof, closed container that is strong enough. Smoking should be prohibited where decaborane is stored or handled. Decaborane is a toxic substance, comparable in this respect to diborane, not less so than pentaborane [22]. Skin contact with decaborane or its solutions should be avoided. Decaborane reacts with natural rubber and destroys latex on contact; buna-nitrile gloves should be used. Alcohol can be used for contamination, followed by a water rinse. A scrubber with active carbon

is effective for decontamination of exhaust from vacuum pumps. Spilled decaborane can be decontaminated with methanol; aqueous ammonia has also been suggested.

Poisoning by decaborane can occur by inhalation, absorption through skin or ingestion, although the possibility of exposure can be minimized by ordinary protection of the skin, the eyes, and the respiratory system. Any decaborane that is splashed or spilled on a person must be thoroughly washed from the affected skin and eyes. Areas containing toxic concentrations of decaborane vapor must be evacuated at once. Whenever there is any kind of decaborane exposure, a physician should be summoned immediately.

Several methods have been developed for the detection and determination of decaborane.It can be determined by ultra-violet spectroscopy in aqueous triethanol-amine solution or colorimetrically from its red adduct with quinoline. Nither diborane nor pentaborane interfere with these methods nor with a calorimetric method based on the orange red solution formed with N, N-diethylinicotinamide.

APPENDIX B

ISOTOPE DISTRIBUTION CALCULATION OF $B_{10}H_{14}$

Naturally occurring Boron contains 19% B^{10} and 81% B^{11}. Boron skeletons of every natural compound contain all possible combinations of B^{10} and B^{11} as governed by binomial distribution:

$$p = (n/k)(p^k)(1-p)^{n-k} \quad (4)$$

Table B1 Isotope distribution of $B_{10}H_{14}$

B_{10}	B_{11}	H	Mass	Probability
0	10	14	124	0.12157
1	9	14	123	0.2309
2	8	14	122	0.301
3	7	14	121	0.18829
4	6	14	120	0.07729
5	5	14	119	0.021756
6	4	14	118	0.004252
7	3	14	117	0.00057
8	2	14	116	0.00005
9	1	14	115	0.0000021
10	0	14	114	0.00000006

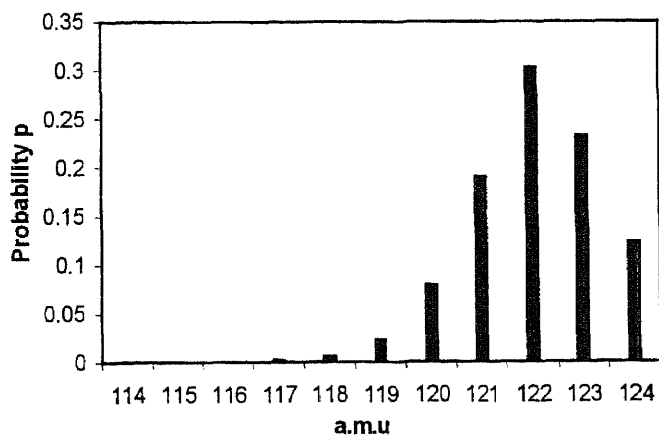

Figure B1 Isotope distribution of $B_{10}H_{14}$

REFERENCES

1. "The National Technology Roadmap for Semiconductors," Semiconductor Industry Association, 1994.

2. Peter Singer, "Ion Implanters: Pushing the Low Energy Limits," *Semiconductor International*, pp. 72-78, April 96.

3. Ruth De Jule, "Meeting the Ultra-Shallow Junction Challenge," *Semconductor International*, pp. 50-54, April 97.

4. Marek Sosnowski, "The Prospects of Low Energy Implantation with Large Molecular Ions- the Case of Decaborane,"- to be published

5. J.F.Zeigler, *Handbook of Ion Implantation Technology*, North-Holland, Amsterdam, 1992.

6. Erin. C. Jones, Emi Ishida, "Shallow junction doping technologies for ULSI," *Materials Science and Engineering*, R24, pp. 1-80, April 1998.

7. Goto.K, Matsuo, J.Sugii, Isao Yamada, and T.Hisatsugu, "Novel Shallow Junction Technology using Decaborane ($B_{10}H_{14}$)," *IEDM-96, IEEE*, pp. 17.1.1-17.1.4, 1996.

8. Jiro Matsuo, Daisuke Takeuchi, Takaaki Aoki and Isao Yamada, "Cluster Ion Implantation for Shallow Junction Formation," *IEEE*, pp. 768-771, 1997.

9. Ken-ichi,Goto, Jiro Matsuo,Yoko Tada, Tetsu Tanaka, Youichi Momiyama, Toshihoro Sugii, and Isao Yamada, "A High Performance 50nm PMOSFET using Decaborane ($B_{10}H_{14}$) Ion Implantation and 2-step Activation Annealing Process," *IEDM-97, IEEE*, pp. 18.4.1-18.4.4, 1997.

10. Wilson Brewer, *Ion Beams with Applications to Ion Implantation*, Wisley Interscience, New York, 1973.

11. F.L.Arnot, *Collision Processes in Gases*, John Wiley and Sons Inc., New York. 1950.

12. Joyce.J.Kaufman, W.S.Koski, L.J.Kuhns and R.W.Law, "Appearance and Ionization Potentials of Selected Fragments from Decaborane, $B^{11}{}_{10}H_{14}{}^{1}$," *J. Am. Chem. Soc*, vol. 84, pp. 4198-4205, 1962.

13. David A. Dahl, *SIMION 3D Version 6.0 user's Manual*, Idaho National Engineering Laboratory Idaho Falls, ID 83415, 1995.

14. Ian.G.Brown, *The Physics And Technology Of Ion Sources*, John Wiley & Sons, New York, 1989.

15. F.Shoji and T.Hanawa, "Ion source constructed from Ionization gauge," *J.Phys.E: Sci.Instrum.* vol.14, pp. 1721-24, 1981.

16. J.Kirschner, "Simple low-energy sputter ion gun based on a Bayard-Alpert pressure gauge," *Rev. Sci. Instrum.*, vol. 57, pp.2640-2642, 1996.

17. Hideo Sugiura, "Simple, high current, antimony ion source", *Rev. Sci. Instrum.*, vol. 50, pp.84, 1979.

18. S.Dworetksy, R.Novick, W.W.Smith, and N.Tolk, "Electron-bombardment ion source," *Rev. Sci. Instrum.*,vol.39, pp.1721, 1968.

19. Russell.J.Hill, *Physical Vapor Deposition*, The BOC GROUP, pp. 17-26, 1996.

20. Steven.K.Krommenhoek, "Design of an Ionized Cluster Beam System for Thin Film Deposition and Cluster Size Measurement," *Thesis, Department of ECE, NJIT* 1990.

21. *eV Parts Manual*, Kimball Physics Inc., Wilton, New Hampshire 03086

22. Hurd, T.Dallas, *An introduction to the chemistry of the hydrides*, Wiley New York 1952.